ACTIVE VIBRATION ISOLATION

FOR FLEXIBLE PAYLOADS

by

Jack D. Leatherwood

Thesis submitted to the Graduate Faculty of the

Virginia Polytechnic Institute

in partial fulfillment for the degree of

MASTER OF SCIENCE

in

Engineering Mechanics

APPROVED:

Chairman: G. W. Swift

F. J. Maher

D. H. Pletta, Head, Engineering Mechanics Department

R. Chicurel

January 1968

Blacksburg, Virginia

ACTIVE VIBRATION ISOLATION FOR FLEXIBLE PAYLOADS

By

Jack D. Leatherwood

Thesis submitted to the Graduate Faculty of the

Virginia Polytechnic Institute

in partial fulfillment for the degree of

MASTER OF SCIENCE

in

ENGINEERING MECHANICS

January 1968

II. TABLE OF CONTENTS

III. ACKNOWLEDGMENTS

The author wishes to express his appreciation to the National Aeronautics and Space Administration which supported the research on which this thesis was written. In addition, the author's thanks are extended to of the Virginia Polytechnic Institute, , and of the Langley Research Center for their encouragement and constructive criticism. The author is also indebted to the many members of the NASA staff who contributed to the preparation and publication of this thesis.

IV. LIST OF FIGURES

V. INTRODUCTION

The protection of equipment and/or personnel from the damaging effects of vibration and shock is a problem repeatedly encountered in equipment design and development. Probably the most common approach to this problem is to isolate the object to be protected from the source of disturbance by a properly designed passive suspension system (soft springs and dampers or viscoelastic mounts, for example). There are, however, two important problems for which passive isolators are unsatisfactory. The first problem arises when the object to be isolated is a low-frequency flexible system whose response to external dynamic disturbances must be kept within certain tolerable limits. The human torso, for instance, has several resonances in the neighborhood of 5 Hz. The second problem occurs when the equipment or personnel is subjected to vibratory and transient loads superimposed upon a gradually changing "steady" acceleration level. When both of these factors occur simultaneously the isolation problem becomes particularly difficult and it is this problem that is considered herein. An example would be the protection of flexible spacecraft payloads where vibratory disturbances are superimposed on the relatively steady flight accelerations which may range typically from 0 to 5 g's. This same phenomenon is also encountered to a degree by aircraft and ground transport vehicles. For example, the passenger compartment of a high-speed ground-based vehicle encounters vibratory disturbances due to roadway irregularities and steady level accelerations due to banking in curves (see ref. 1).

Normal roadway irregularities include both low amplitude, short wavelength components due to construction tolerances, and so forth, as well as longer wavelength, larger amplitude components due to terrain profile, foundation shifts, and so forth. Passive isolators are not suitable for systems of this type because of the large static deflections associated with changes in steady acceleration level. Thus, an analytical and experimental investigation has been initiated to determine the feasibility of using an automatically controlled (active) vibration isolation system.

Various active isolation systems utilizing controllable viscous dampers have been investigated in the literature (see refs. 2 and 3). These provide very good isolation characteristics under a 1-g acceleration but are unsuitable for launch vehicle application since they behave as a passive system under static loading conditions. Other active vibration control techniques incorporate the use of servomechanisms to eliminate isolator static deflections (see refs. 4 and 5. These systems are primarily used for rigid-body isolation where a fixed reference for measuring payload displacement is readily available.

This paper presents the results of a research investigation to determine the feasibility of using an active vibration isolation system to protect sensitive, nonrigid payloads from the combined steady and vibratory load environment. For purposes of illustration and discussion the problem of launch vehicle payload isolation will be considered although the results are applicable to other problems such as passenger compartment isolation. The approach used is to provide

an "isolation interface" between a launch vehicle and its payload that will (1) significantly attenuate the response of the payload to vibration disturbance generated in the launch vehicle and transmitted through the interface and (2) damp the payload response to transient loads such as those generated during booster staging or control maneuvers. The vibration isolator developed in this study is an active system that measures the local response of a low-frequency nonrigid payload and introduces forces to cancel this response. The active vibration isolation system consists of: (1) sensing elements to measure payload response, (2) control networks to process the measured response signals, and (3) a variable force actuating element that responds to the control commands in such a manner as to null the payload response. Primary consideration is given to the problem of isolating a single-degree-of-freedom payload although some preliminary work is included to indicate the possible extension of this approach to payloads with more than one degree of freedom. Analog and digital computer studies of the isolation system are conducted and a working model of the isolator is developed. Theoretical and experimental results in the form of transmissibility and transient response plots are presented to indicate the effectiveness of this isolator in attenuating the response of a one-degree-of-freedom payload to steady state and transient vibratory disturbances. Preliminary results are also included to illustrate the potential application of the isolator to the problem of isolating a two-degree-of-freedom payload.

VI. LIST OF SYMBOLS

A parameter defined by equation (29), sec^{-2}

A_p piston area, in^2

a constant defined by equation (36), sec^{-1}

B parameter defined by equation (30), sec^{-2}

b constant defined by equation (37), sec^{-2}

C parameter defined by equation (31), sec^{-2}

C_a accelerometer sensitivity, volts/in./sec^2

C_f sensitivity of actuator piston position sensor, volts/in.

C_m damping coefficient (single mass payload) $\frac{\text{lb-sec}}{\text{in.}}$

C_o constant relating valve spool displacement to error voltage, in./volt

C_v constant relating actuator flow to valve spool displacement, in^2/sec

C_1, C_2 damping coefficient, upper and lower mass, respectively, $\frac{\text{lb-sec}}{\text{in.}}$

c constant defined by equation (38), sec^{-3}

D parameter defined by equation (32), sec^{-2}

d constant defined by equation (39), sec^{-4}

E_o output of potentiometer, volts

e constant defined by equation (40), sec^{-5}

F_e external force applied to payload mass, lb

F_o steady force acting on payload, lb

f_n natural frequency, Hz

$G(s)$ forward loop transfer function (eq. (15))

$G_1(s)$ equivalent transfer function (see eq. (22))

$H_1(s)$, $H_2(s)$, $H_3(s)$ feedback loop transfer functions (eqs. (19), (20), and (21), respectively)

j denotes complex number, $j = \sqrt{-1}$

K spring constant, lb/in.

K_o spring constant, lb/in.

K_1, K_2 spring constant, upper and lower mass, lb/in.

k_c feedback control gain, sec^2

k_m spring constant (single D.O.F. payload), lb/in.

M mass, lb-sec^2/in.

M_1, M_2 upper and lower mass, lb-sec^2/in.

Q volume flow rate, ft^3/sec

s laplace transform variable, sec^{-1}

T transmissibility

$\bar{t}$ time to damp to one-half amplitude, sec

t_o time to damp to one-half amplitude for $k_c = 0$, sec

W weight, lb

w relative displacement, in.

x payload mass displacement, in.

x_v servo valve displacement, in.

x_1, x_2 upper and lower mass displacement, respectively, in.

y actuator piston displacement, in.

z input disturbance displacement, in.

α	axial acceleration, g units
γ	normalized damping time, $\bar{t}/t_o$
Δ	static deflection, in.
ϵ	error voltage, volts
δ	servo valve control signal, volts
δ_a	accelerometer output, volts
ζ	damping ratio (two-degree-of-freedom payload)
ζ_o	accelerometer damping ratio
ζ_m	damping ratio (single-degree-of-freedom payload)
λ	payload overshoot, see equation (42)
σ	real part of s, $s = \sigma + j\omega$
τ	time constant (lead network), sec
τ_a	time constant (actuator), sec
τ_l	time constant (lag network), sec
ω	natural circular frequency, rad/sec
ω_m	payload natural frequency, rad/sec
ω_o	accelerometer natural frequency, rad/sec

VII. CHOICE OF ISOLATOR SYSTEM

Isolator Requirements

The problem of payload isolation is presented schematically in figure 1 which shows a flexible payload mounted to a launch vehicle. For illustrative purposes it is assumed that the launch vehicle is a source of longitudinal vibration input, $\ddot{z}(t)$, and the acceleration response of the flexible payload is defined as the output and is denoted by $\ddot{x}(t)$. The objective, then, is to provide a vibration isolation system at the payload-launch vehicle interface that will effectively attenuate payload response to vibratory disturbances transmitted through the isolator and transient disturbances acting directly on the payload. There are three very important conditions under which the isolator must operate. These are:

(1) Both the payload and the launch vehicle are assumed to have critical frequencies which are less than 10 Hz. Thus the isolator must be capable of minimizing the low-frequency, large-amplitude response of such structures.

(2) The isolator must operate within a variable "steady state" or nonvibratory acceleration field ranging from 1 to 5 g's.

(3) "Rattle space" for payloads is generally very limited, therefore the isolator itself must maintain a fixed position.

Vibration isolation systems are generally categorized as being either passive or active. Passive isolation systems depend entirely upon the dynamic characteristics of passive elements, such as

mechanical springs and viscous dampers, for the required vibration isolation. Active systems, however, employ automatically controlled or active elements to sense the disturbance response and introduce forces to oppose it. The following paragraphs discuss the characteristics of both the passive and active vibration isolation systems.

Passive Isolation Systems

For most conventional (or 1g) vibration isolation problems the object to be isolated is mounted on relatively soft springs and dampers. A typical example is the automobile. This approach, however, has certain limitations when applied to the problem of payload isolation. A review of the characteristics of a passive isolation system (refs. 6 and 7) will readily verify this point. Figure 2 illustrates schematically a rigid payload being isolated from a moving support by a passive isolator consisting of a spring and viscous damper. The transmissibility of the system is defined as the ratio of output acceleration to input acceleration and is presented as a function of frequency ratio, that is, input (or driving) frequency divided by the natural frequency of the isolator. Transmissibility plots are shown for the case where the damping ratio, C/C_c, is zero and 0.2. The transmissibility is large when the driving frequency, ω, is near the natural frequency of the isolation system, ω_n. This corresponds to a frequency ratio of approximately 1. For values of frequency ratio above $\sqrt{2}$ the transmissibility becomes increasingly less than 1. If, for the case shown in figure 2, an 80-percent reduction in vibration response is desired

(transmissibility = 0.20) the frequency ratio must be equal to or greater than 5. Thus, if the input frequency of the launch vehicle is 5 Hz, the isolator must be designed to have a natural frequency of 1 Hz. The inherent problem with a soft system of this nature is the large static deflections that result if the "steady" acceleration level changes. The static deflection, Δ, is defined as

$$\Delta = \frac{F_o}{K} \tag{1}$$

where F_o is the steady force acting on the payload and K is the spring constant. For this problem

$$F_o = \alpha W \tag{2}$$

where α denotes the number of g units and W is the weight of the payload. For a spring-mass system, neglecting damping, the natural frequency is given by

$$f_n = \frac{1}{2\pi} \sqrt{\frac{K}{M}} \tag{3}$$

where M is the mass of the payload. Substituting (2) and (3) into (1) gives the following expression for static deflection.

$$\Delta = \frac{9.78\lambda}{f_n^2} \tag{4}$$

Equation (4) is plotted in figure 3 for a 1-Hz isolation system. As indicated by figure 3, a 1-Hz system has a static deflection of approximately 10 inches under a steady acceleration of 1g. When the longitudinal acceleration is increased, the static deflection becomes much larger. The deflection associated with a 5-g acceleration, for example, is approximately 50 inches which is obviously undesirable.

Active Vibration Isolation System

In order to minimize both vibration and static deflection under conditions of varying acceleration, it is apparent that some form of an automatically controlled isolation system is required. This involves the establishment of control criteria, the selection of the important control or response variables, the measurement of the control variables, the processing of the measurements through a feedback compensation network, and the utilization of the processed values to operate an actuating element in such a manner as to satisfy the control criteria. A schematic diagram of the active isolation system selected is shown in figure 4, the components of which are discussed in the following paragraphs.

Actuating Element

The actuating element must be capable of generating and applying a variable force to the payload in response to control commands. Such elements are available in the form of servo-driven pneumatic or hydraulic actuators. An electrohydraulic servo actuator was chosen

because it offers several distinct advantages over the corresponding pneumatic actuators. Among these are:

(1) Hydraulic cylinders are essentially linear elements since the compressibility effects of the oil are usually negligible. Pneumatic cylinders, on the other hand, are generally nonlinear due to the compressibility effects of air.

(2) Hydraulic systems can respond quicker than pneumatic systems. Pneumatic systems cannot respond until the effects of compressibility have taken place.

(3) The inherent nonlinearities of pneumatic systems create a more complex design problem. Therefore, they cannot readily handle changes in system parameters without redesign efforts.

Control Criteria and Control Variables

The control variables are obviously the absolute acceleration of the payload and the isolator static deflection. These will be measured by suitable acceleration and displacement transducers. The control criteria are simply to (1) maintain the vibratory accelerations of the payload at a zero level, and (2) eliminate isolator static deflection. It is important to keep in mind the fact that the payload itself will still "see" and (since it is flexible) respond to the steady acceleration levels, that is, it will deflect due to the variations in flight acceleration level.

Compensation Networks

The compensation networks consist of an acceleration controller to process the measured acceleration signal and a position controller to process the measured isolator deflection signal. Two modes of acceleration control are considered. The first mode, called mode I, consists of proportional lead-lag compensation, and the second mode, mode II, consists of lead compensation only. The lead network is used to eliminate the response of the isolator to the DC acceleration component and the lag network attenuates the high-frequency components of the measured acceleration signal.

The position controller is simply a direct proportional feedback of isolator displacement.

VIII. PRESENTATION OF ANALYTICAL RESULTS

General

This section presents the results of an analytical investigation to determine the effectiveness of the active isolation system in protecting a low-frequency, single-degree-of-freedom payload. The analytical model of the isolator system is described and the system transfer functions are developed. Digital and analog computer studies are then made to obtain the transmissibility and transient response characteristics of the system. Preliminary analog computer results are presented for a two-degree-of-freedom payload to illustrate the possible application of the active isolator to more complex payloads.

Analytical Model

The various components of the analytical model of the isolator-payload system are shown in figure 4. The payload is represented by a one-degree-of-freedom spring-mass-damper system tuned to have a resonant frequency of 30 rad/sec or 4.87 Hz and is shown suspended from the top of a rigid box that is in turn rigidly fastened to the hydraulic actuator piston. It is assumed that this payload model is typical of the fundamental resonant response characteristics of a discrete or continuous structure, and also that the higher resonances, if present, are much less critical. The justification for these assumptions is based on the fact that the principal danger to payloads of this nature arises from the large amplitudes associated with

low-frequency response. Also, the isolation of the payload from the high-frequency disturbances can generally be handled by more conventional techniques.

The operation of the active vibration isolator is described as follows: (1) the vibratory response of the payload to launch vehicle disturbance vibrations, $\ddot{z}(t)$, and/or external disturbances, $F(t)$, is measured by a servo accelerometer. The external disturbance function includes the force due to a steady flight acceleration. Thus, the servo accelerometer generates a signal proportional to the superposition of payload acceleration response and steady flight acceleration, (2) the acceleration signal is applied to the acceleration controller for compensation. During this process the lead network eliminates the steady (or DC component) of the signal, (3) the output of the acceleration controller is amplified and applied to the servo valve, resulting in flow through the valve that is proportional to the payload acceleration, and (4) the servo valve displacement generates an actuator piston velocity, causing the piston to move to oppose the payload acceleration. It is important to note that the servo actuator response to the compensated acceleration error signal is an approximate integration process. Thus, the actuator force applied to the payload is approximately proportional to payload velocity. This corresponds to the addition of damping to the system. A second loop measures the actuator piston position, compares it to a preset command position, and generates a signal to the servo valve that tends to restrict the piston to move

about the command position. It is this loop, together with the lead network, that eliminates isolator response to gradually changing steady acceleration levels.

System Transfer Functions

The signal flow diagram of the payload-isolator system is presented in figure 5. The transfer functions associated with each block of the signal flow diagram will now be discussed.

A sketch of the payload model and the coordinate system used to develop its transfer function is shown in sketch 1.

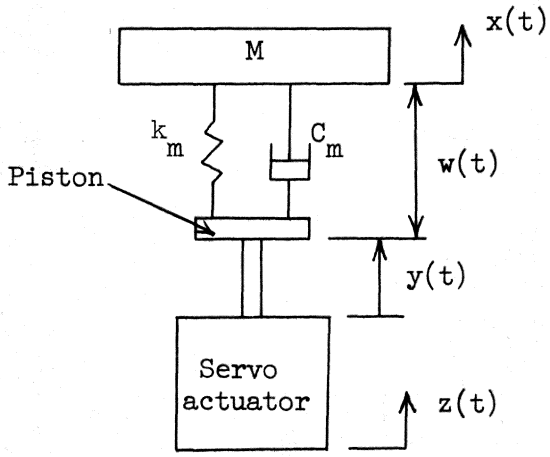

Sketch 1. Payload model and coordinate system

The x and z coordinates are independent. The y coordinate defines the position of the actuator piston relative to the actuator housing and the w coordinate is the relative displacement between the payload mass and the payload support structure. Summing the forces acting on the payload mass gives

$$M\ddot{x} = -k_m w - C_m \dot{w} \tag{6}$$

or

$$\ddot{x} = -\frac{1}{M}\left[k_m w + C_m \dot{w}\right] \tag{7}$$

Taking the laplace transform of equation (7) results in

$$x(s) = -\frac{1}{M}\left[k_m + C_m s\right] w(s) \tag{8}$$

where s is the laplace transform variable. Rearranging

$$\frac{x(s)}{w(s)} = -\frac{1}{M}\left[k_m + C_m s\right] \tag{9}$$

Equation (9) is the transfer function relating the acceleration response of the flexible payload to the input disturbance displacement.

In order to develop an approximate servo actuator transfer function, the following simplifying assumptions are made:

(a) The hydraulic oil is incompressible.

(b) Servo valve spool displacement is directly proportional to actuating voltage.

(c) Servo valve flow is directly proportional to the valve spool displacement.

Consistent with these assumptions the block diagram of the servo actuator with closed-loop position control is represented as shown in sketch 2.

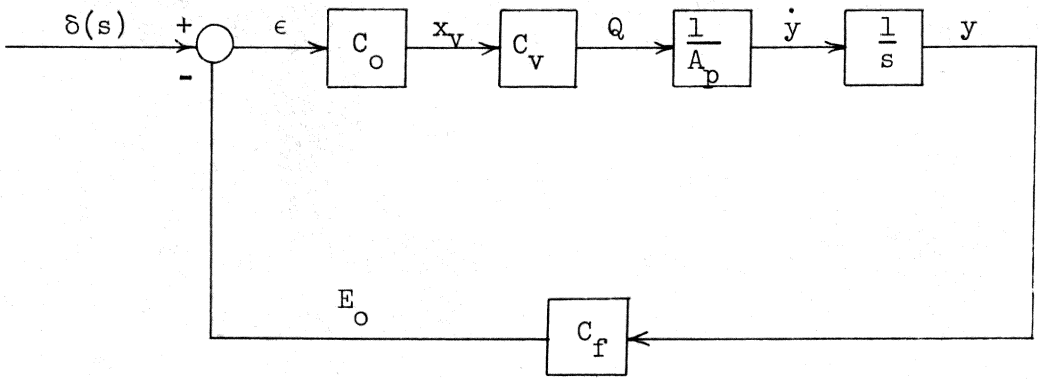

Sketch 2

From sketch 2, the transfer function relating piston displacement, y, to actuating voltage, δ, can be written. It is

$$\frac{y(s)}{\delta(s)} = \frac{1}{C_f}\left(\frac{1}{\frac{A}{C_o C_v C_f}s + 1}\right)$$

or

$$\frac{y(s)}{\delta(s)} = \frac{1}{C_f}\left(\frac{1}{\tau_a s + 1}\right) \tag{10}$$

where

$$\tau_a = \frac{A}{C_o C_v C_f} \tag{11}$$

and C_o is the constant relating valve spool displacement to error voltage ϵ, C_v is the constant relating actuator flow to valve spool displacement, A is the piston area, Q is volume flow through valve, y is the actuator piston displacement, and C_f is the constant that

converts piston displacement to an equivalent voltage. The constant, τ_a, is the time constant of the servo actuator and has the value of 0.40 sec. The constant, C_f, has the value of 60 volts/in.

The mode I acceleration controller consists of a lead-lag compensation network with overall gain k_c. The transfer function in laplace operator notation is

$$\frac{\delta(s)}{\delta_a(s)} = k_c \left(\frac{\tau s}{\tau s + 1}\right) \left(\frac{1}{\tau_1 s + 1}\right) \tag{12a}$$

where δ is the output of the acceleration controller and τ and τ_1 are time constants and are set equal to one ($\tau = \tau_1 = 1.0$).

The mode II acceleration controller consists of lead compensation only and its transfer function is

$$\frac{\delta(s)}{\delta_a(s)} = k_c \left(\frac{\tau s}{\tau s + 1}\right) \tag{12b}$$

The transfer function of the servo accelerometer is

$$\frac{\delta_a(s)}{\ddot{x}(s)} = \frac{C_a}{\frac{s^2}{\omega_o^2} + \frac{2\zeta_o}{\omega_o} + 1} \tag{13}$$

where ω_o is the natural frequency of the accelerometer and ζ_o is the accelerometer damping ratio, and C_a is the sensitivity of the accelerometer. The accelerometer used in this study has a natural frequency of 300 Hz (ω_o = 1885 rad/sec) and a damping ratio of

approximately 0.7. Consequently, for the operating frequencies considered in this study, the transfer function is

$$\frac{\delta_a(s)}{\ddot{x}(s)} = C_a \tag{14}$$

The block diagram of the active isolation system with the appropriate transfer functions substituted is shown in figure 6. The mode I and mode II acceleration controllers are indicated by the dashed boxes and are mutually exclusive.

Digital Computer Study

The NASA-Langley IBM 7094 was utilized to compute the transmissibility and stability characteristics of the active isolator system with the one-degree-of-freedom payload model. For convenience the transmissibility is defined as the ratio of payload velocity, $\dot{x}$, to input disturbance velocity, $\dot{z}$. The block diagram used to develop the transmissibility equation is given in figure 7. The forward loop transfer function ahead of the acceleration pickoff point is defined as

$$G(s) = \frac{1}{M}\left(\frac{k_m}{s} + C_m\right) \tag{15}$$

Setting

$$\frac{k_m}{M} = \omega_m^2 \tag{16}$$

and

$$\frac{C_m}{M} = 2\zeta_m \omega_m \tag{17}$$

results in

$$G(s) = \frac{\omega_m^2}{s} + 2\zeta_m \omega_m \tag{18}$$

The inner feedback loop transfer function for mode I acceleration control is

$$H_1(s) = \frac{s^2 k_c \tau C_a}{(\tau_a s + 1)(\tau s + 1)(\tau_1 s + 1)(C_f)} \tag{19}$$

and for mode II control is

$$H_2(s) = \frac{s^2 k_c \tau C_a}{(\tau_a s + 1)(\tau s + 1)(C_f)} \tag{20}$$

The outer feedback loop transfer function is

$$H_3(s) = 1 \tag{21}$$

The block diagram of figure 7 can now be replaced by the system illustrated in sketch 3.

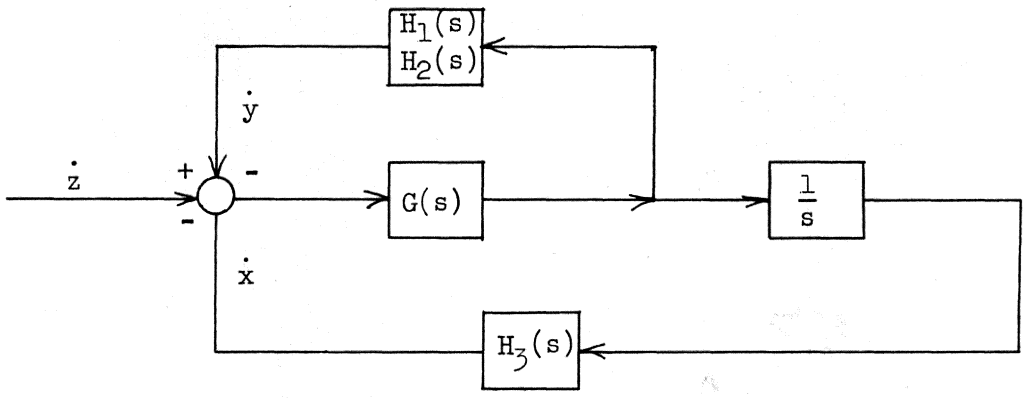

Sketch 3

The block diagram can be further simplified by replacing the inner feedback loop of sketch 3 by its equivalent transfer function, which is

$$G_1(s) = \frac{G(s)}{1 + G(s)H(s)} \tag{22}$$

where $H(s)$ can be either of the acceleration controller transfer functions. The block diagram now reduces to that indicated by sketch 4.

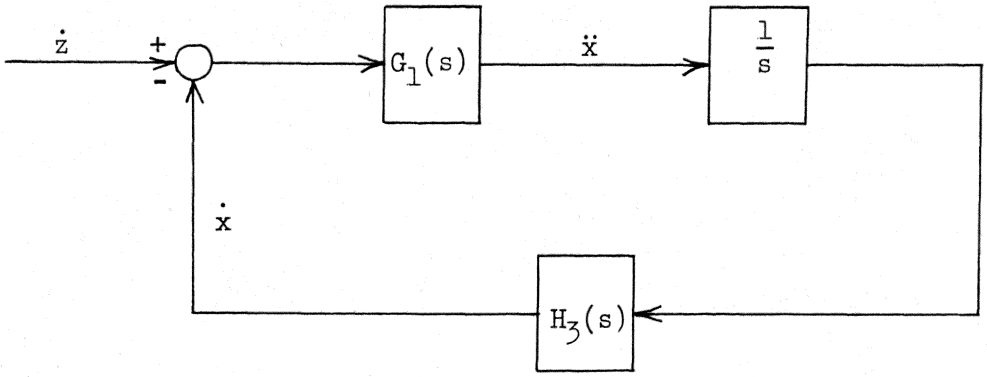

Sketch 4

Using sketch 4, the transmissibility equation can be written directly. It is

$$\frac{\ddot{x}(s)}{\ddot{z}(s)} = T(s) = \frac{\dfrac{G_1(s)}{s}}{1 + \dfrac{1}{s} G_1(s)H_3(s)} \tag{23}$$

or

$$T(s) = \frac{G_1(s)}{s + G_1(s)H_3(s)} \tag{24}$$

Substituting the appropriate transfer functions for the case of mode I control gives

$$T(s) = (2\zeta_m \omega_m s + \omega_m^2)(\tau_a s + 1)(\tau_1 s + 1)(\tau s + 1)(C_f) \Big/ (C_f)^2(\tau_a s + 1)(\tau_1 s + 1)(\tau s + 1) + (2\zeta_m \omega_m s + \omega_m^2)k_c \tau C_a s^3 + (2\zeta_m \omega_m s + \omega_m^2)(C_f)(\tau_a s + 1)(\tau_1 s + 1)(\tau s + 1) \tag{25}$$

For steady-state vibrations the laplace transform variable can be replaced by

$$s = j\omega \tag{26}$$

Equation (25) now becomes

$$T(j\omega) = (\omega_m^2 + 2j\zeta_m \omega_m \omega)(1 + j\tau_a \omega)(1 + j\tau\omega)(1 + j\tau_1 \omega)(C_f) \Big/ (C_f)(\omega^2)(1 + j\tau_a \omega)(1 + j\tau\omega)(1 + j\tau_1 \omega) + (\omega_m^2 + j2\zeta\omega_m \omega)k_c \tau C_a(-j\omega^3) + (\omega_m^2 + j2\zeta_m \omega_m \omega)(C_f)(1 + j\tau_a \omega)(1 + j\tau\omega)(1 + j\tau_1 \omega) \tag{27}$$

Equation (27) can be written in the form

$$T(j\omega) = \frac{A + jB}{C + jD} \tag{28}$$

where

$$A = \omega_m^2\left[1 - \omega^2(\tau_a\tau_1 + \tau_a\tau + \tau_1\tau)\right] - 2\zeta_m\omega_m\omega\left[\omega(\tau_a + \tau_1 + \tau) - \omega^3\tau_a\tau_1\tau\right] \tag{29}$$

$$B = \omega_m^2\left[\omega(\tau_a + \tau_1 + \tau) - \omega^3\tau_a\tau_1\tau\right] + 2\zeta_m\omega_m\omega\left[1 - \omega^2(\tau_a\tau_1 + \tau_a\tau + \tau_1\tau)\right] \tag{30}$$

$$C = \omega_m^2\left[1 - \omega^2(\tau_a\tau_1 + \tau_a\tau + \tau_1\tau)\right] - 2\zeta_m\omega_m\omega\left[\omega(\tau_a + \tau_1 + \tau) - \omega^3\tau_a\tau_1\tau\right] - \omega^2\left[1 - \omega^2(\tau_a\tau_1 + \tau_a\tau + \tau_1\tau\right] + 2k_c\tau\zeta_m\omega_m\omega^4\frac{C_a}{C_f} \tag{31}$$

$$D = \omega_m^2\left[\omega(\tau_a + \tau_1 + \tau) - \omega^3\tau_a\tau_1\tau\right] + 2\zeta_m\omega_m\omega\left[1 - \omega^2(\tau_a\tau_1 + \tau_a\tau + \tau_1\tau)\right] - \omega^2\left[\omega(\tau_a + \tau_1 + \tau) - \omega^3\tau_a\tau_1\tau\right] - k_c\tau\omega_m^2\omega^3\frac{C_a}{C_f} \tag{32}$$

Finally, the transmissibility can be calculated as a function of input frequency ω by determining the magnitude of $T(j\omega)$

$$\left|T(j\omega)\right| = T = \sqrt{\frac{A^2 + B^2}{C^2 + D^2}} \tag{33}$$

and the phase angle is

$$\Phi = \tan^{-1}\frac{B}{A} - \tan^{-1}\frac{D}{C} \tag{34}$$

Equation (33) represents the transmissibility of the active isolator with a one-degree-of-freedom payload for mode I acceleration feedback control. This equation was programed on the digital computer for calculation of transmissibility as a function of the ratio of input frequency to payload natural frequency. The results of the transmissibility calculations are presented in figure 8 which is a plot of transmissibility versus frequency ratio for various values of feedback loop gain k_c for mode I control. The curve for $k_c = 0$ is the steady-state response of the payload without active control. The upper limit on the control gain is $k_c = 924$ since for values slightly larger than this the control system becomes unstable. The isolation characteristics are good for the lower frequency range $(\omega/\omega_m \lesssim 1.5)$, especially at the resonant frequency of the payload. However, for the higher frequencies the transmissibility curves (with the exception of the case for $k_c = 924$ indicate some deterioration of isolation capability when compared to the no-control condition.

Stability was investigated by calculating the roots of the characteristic equation obtained from the denominator of the closed-loop transfer function of the system. The characteristic equation is defined by the denominator of equation (25) and is

$$s^5 + as^4 + bs^3 + cs^2 + ds + e = 0 \tag{35}$$

where

$$a = \frac{\tau_a\tau_1 + \tau_a\tau + \tau_1\tau + 2\zeta_m\omega_m k_c\tau + 2\zeta_m\omega_m\tau_a\tau_1\tau}{\tau_a\tau_1\tau} \tag{36}$$

$$b = \frac{\tau_a + \tau_1 + \tau + \omega_m^2 k_c\tau\left(\frac{C_a}{C_f}\right) + 2\zeta_m\omega_m(\tau_a\tau_1 + \tau_a\tau + \tau_1\tau) + \omega_m^2\tau_a\tau_1\tau}{\tau_a\tau_1\tau} \tag{37}$$

$$c = \frac{1 + 2\zeta_m\omega_m(\tau_a + \tau_1 + \tau) + \omega_m^2(\tau_a\tau_1 + \tau_a\tau + \tau_1\tau)}{\tau_a\tau_1\tau} \tag{38}$$

$$d = \frac{2\zeta_m\omega_m + \omega_m^2(\tau_a + \tau_1 + \tau)}{\tau_a\tau_1\tau} \tag{39}$$

$$e = \frac{\omega_m^2}{\tau_a\tau_1\tau} \tag{40}$$

The roots of equation (35) were calculated as a function of feedback gain k_c and the results for the control mode are presented in figure 9 in the form of a root locus plot for the positive frequency values only. For very small feedback gains, $k_c \leq 0.693$, the control

mode behaves essentially as a nonoscillatory system. At the value $k_c \approx 1.155$ the root locus breaks away from the negative real axis, thus becoming oscillatory and at the value $k_c = 23.1$ begins to become less stable for increasing loop gain. At a value of feedback gain slightly larger than 924 the locus crosses the imaginary axis into the real plane, signifying an unstable condition.

For mode II control the first-order time lag is removed by setting $\tau_1 = 0$ in equation (27). The transmissibility and stability calculations are performed as before and the results are presented in figure 10 and figure 11, respectively. Figure 10 indicates a marked improvement in transmissibility over the entire frequency range for much lower values of feedback gain. The root locus plot (fig. 11) for the unstable root shows that the instability occurs for much lower values of feedback gain. With these results in mind, an analog computer study of the simulated active isolation system was conducted for the mode II feedback control system only.

Analog Computer Results

One-degree-of-freedom model.- The analog computer is a very useful and versatile tool and is especially suited for investigations of this nature. It pprovides a means of rapidly determining the effect of variations of individual system parameters on overall system performance as well as permitting the simulation of a gradually changing steady acceleration level. In addition, the isolator response to sinusoidal, step, or impulsive input disturbances can be observed and

evaluated in real time. The particular computer used for this study is a Pace Model 231R.

The analog computer circuit diagram representing the block diagram of figure 7 for mode II acceleration control is illustrated in figure 12. The input disturbance functions are applied to integrator 06 and the acceleration response of the payload is picked off the output of amplifier 22.

This signal is then applied to the lead network with feedback gain set by attenuator Q_{15}. The output of the lead network drives the simulated servo actuator to generate the actuator piston velocity, $\dot{y}$, at the output of amplifier 17. The piston velocity is integrated once to obtain piston displacement which is fed back through attenuator Q_{17} to amplifier 17. The piston velocity is then applied to the input of integrator 06 to complete the acceleration feedback loop. The time constants for the controller and actuator are set at the same values used in the digital computer simulation.

The results of the transmissibility calculations using the analog computer are identical to those obtained in the digital computer simulation (fig. 10). To obtain the transient response characteristics of the active isolation system to simulated step acceleration inputs it is necessary to analytically generate the servo actuator piston acceleration. This is accomplished by representing the servo actuator as a highly damped second-order system as shown in the analog computer circuit diagram of figure 13. The analog computer plots of figure 14

illustrate typical transient response characteristics of the payload-isolator system to a 1.0-g step input acceleration.

The input disturbance acceleration is shown on the upper trace, the payload acceleration response on the middle trace, and the actuator piston displacement on the lower trace. Figure 14(a) shows the response of the system for the "control-off" condition. The payload responds as a lightly damped system at a frequency of approximately 4.87 Hz. Figures 14(b), 14(c), and 14(d) show the effect of increasing feedback gain on system response. Note, particularly, the highly damped payload response and the quick return of the actuator piston to its preset position. However, this improved performance is accomplished at the expense of larger piston deflections. Thus, the upper limit of isolator performance will be highly dependent upon the physical limitations of the actuator (total stroke, for example). Ths piston displacements and actuator response time can be reduced by setting the position feedback gain at higher values. This, in turn, limits the ability of the servo actuator to respond freely to control commands. Thus, the design of an isolation system of this nature will have to consider the performance trade-off's between tight position control of the isolator and tight acceleration control of the payload.

The transient response data are summarized in figure 15 which presents the variation of the normalized damping time and payload overshoot with acceleration feedback gain k_c. Normalized damping time and overshoot are defined as follows:

$$\Delta = \text{normalized damping time} = \frac{\bar{t}}{t_o} \tag{41}$$

where $\bar{t}$ is the time required for the payload to damp to one-half amplitude with control on and t_o is the corresponding damping time for the control-off condition.

$$\lambda = \text{overshoot} = \frac{|\ddot{x}| - |\ddot{z}|}{|\ddot{z}|} \tag{42}$$

Examination of figure 15 indicates a very rapid initial decrease in damping time and an appreciable decrease in payload overshoot for increasing gain values. For $k_c > 5.0$ the damping time remains essentially constant and the primary effect of the control system is a reduction in payload overshoot.

A slowly varying steady acceleration level was simulated by applying a low-level DC voltage to the input of an integrator and thence to the input of amplifier 22. The resulting steady state and transient response behavior of the system was unchanged.

Active Isolator and Two-Degree-of-Freedom Payload

This section presents the preliminary results of a study to evaluate the potential ability of the active isolator to attenuate the flexible response of a more complex payload. This payload is represented by the two-degree-of-freedom model shown in figure 16. The equations of motion for the payload with no control are:

$$\ddot{x}_2 = -\frac{K_2}{M_2}(x_2 - z) - \frac{C_2}{M_2}(\dot{x}_2 - \dot{z}) - \frac{K_1}{M_2}(x_2 - x_1) - \frac{C_1}{M_2}(\dot{x}_2 - \dot{x}_1) \tag{43}$$

and

$$\ddot{x}_1 = -\frac{K_1}{M_1}(x_1 - x_2) - \frac{C_1}{M_1}(\dot{x}_1 - \dot{x}_2) \tag{44}$$

Setting $C_1 = C_2 = C$, $K_1 = K_2 = K$, $z = 0$, and $M_1 = M_2 = M$ and using the relations

$$\frac{K}{M} = \omega^2 = 900 \text{ rad/sec}^2 \tag{45}$$

and

$$C/M = 2\zeta\omega = 0.10 \text{ sec}^{-1} \tag{46}$$

the undamped coupled natural frequencies of the model can be calculated. They are $f_1 = 2.91$ Hz and $f_2 = 7.72$ Hz. The analog circuit diagram representing equations (41) and (42) is shown in figure 17. It is assumed that only one acceleration measurement is available and this is arbitrarily chosen to be the acceleration of mass M_2. Using the same active isolation system as before the transmissibility curves of figure 18(a) and figure 18(b) were obtained. Figure 18(a) shows the response of the lower mass (M_2) for the "no-control" and "control-on" conditions. Figure 18(b) indicates the response of the upper mass. Both figures show a significant reduction in transmissibility over the frequency range with the exception of the point at 5 Hz. At this

frequency, the isolator seems to have relatively little effect on the system.

The response of the payload and isolator to a 1-g step acceleration disturbance is presented in figure 19. The response of both masses is quickly damped, but at the expense of somewhat large piston displacements and a much slower return to the preset position.

IX. PRESENTATION OF EXPERIMENTAL RESULTS

General

Experimental models of the active isolation system and single-degree-of-freedom payload were built to provide data for comparison with the analytical results. The experimental data are presented in two forms. First, the actual isolator hardware is applied to the problem of isolating an analog computer simulation of the payload. The disturbance inputs for this case are sinusoidal and step accelerations. Secondly, the isolation system hardware is used to isolate an actual physical model of the payload. This model is comprised of leaf springs and a cylindrical mass and is tuned to have a resonant frequency of 4.82 Hz. The disturbance inputs for this case are sinusoidal and step displacements. Displacement inputs are used because of the difficulty of experimentally generating a step acceleration.

Experimental Active Isolator Model

The experimental model of the active isolator consists of: (1) a servo accelerometer to measure payload response, (2) a proportional lead network (acceleration controller) to process the output signal from the servo accelerometer, (3) a linear potentiometer to measure piston displacement, (4) a direct proportional network (position controller) to process the output signal from the potentiometer, and (5) an electrohydraulic servo actuator to apply a variable force to the payload in response to control commands.

The input vibration disturbances are applied to the experimental payload by means of a hydraulic vibration exciter system.

The servo accelerometer is a Kistler model 303B. It has a natural frequency of 300 Hz with a flat frequency response from DC to 100 Hz. The electrohydraulic servo actuator is a surplus item originally intended for use as a control fin actuator on the NASA Scout launch vehicle. It is a 3000-psi device capable of generating a force up to 1500 pounds with a total stroke of 1 inch. Frequency response tests indicate a reasonably flat frequency response up to approximately 12 cps. The servo valve is a flow control device with full rated flow (0.38 ± 15 percent G.P.M.) at 8 ma differential current and 1000 psi differential pressure. The acceleration controller is the same as that discussed in the analysis section for mode II control and is shown in figure 6. The operational amplifiers of the analog computer were used to build the control functions. A photograph of the experimental isolator and model is shown in figure 20 with the various components labeled. The electrohydraulic servo actuator is shown mounted between the hydraulic vibration exciter and payload.

Experimental Results

The experimental data are presented in figure 21 which is a plot of transmissibility versus frequency ratio. The unshaded symbols indicate the results obtained by using the experimental isolator to attenuate the response of the simulated payload. The upper and lower curves correspond to feedback gains of 2.31 and 23.1, respectively.

Both curves show very good isolation capability for values of frequency ratio less than 2.0. For frequency ratios greater than 2.0 the data tend to approach or exceed the "control-off" curve. This is believed to be due to the combined effect of actuator response dropoff and phase shift in the 10- to 12-Hz region. The important point, however, is the fact that the transmissibility is substantially less than one over the entire frequency range investigated, particularly at the payload resonant frequency. The shaded symbols represent the best data obtained by using the experimental payload model. These data compare favorably with the data obtained with the simulated payload although the same degree of isolation was not attainable at the higher frequencies. The feedback gain for this case was approximately two-thirds the value used with the simulated payload.

The transient response of the simulated payload to a step-input acceleration is shown in figure 22(a) for the "control-off" condition and in figure 22(b) for the "control-on" condition. With control the payload response is damped out in less than one cycle and the actuator piston quickly returns to the preset position.

A comparison of the analytical and experimental results (for the simulated payload) is presented in figure 23 for two values of acceleration feedback gain. The experimental data compare favorably with the theoretical curves, especially in the region near payload resonance. Keeping in mind the linear analytical approximations of the physical system components, this is felt to be very good agreement.

X. CONCLUDING REMARKS

An experimental and analytical investigation has been conducted to determine the feasibility of using an automatically controlled vibration isolation system for protection of flexible payloads from dynamic disturbances inputs. Based on the results of the investigation, the following statements can be made:

(1) The feasibility of such a system has been proven and its effectiveness verified by experimental tests of an active isolator model.

(2) The active isolation system has the ability to sense the local dynamic response of a nonrigid payload and utilize this measurement to generate forces that oppose the response.

(3) The steady-state response, or transmissibility, of a single-degree-of-freedom payload isolator system can be held to a low level over a range of frequencies. The transmissibility never exceeded one and in most cases was substantially less than one.

(4) In the higher frequency range ($\omega/\omega_m \geq 2.0$) the isolator had negligible effect on the transmissibility characteristics of the system.

(5) The active isolation system was highly effective in damping the transient response of the payload to step disturbances.

(6) The preliminary results for the two-degree-of-freedom payload suggest an effective application of the active isolator to more complex payloads.

(7) The static deflection of the isolator due to a gradually changing steady acceleration level is negligible.

(8) Further work should be done to define the performance capabilities with respect to the isolation of more complex discrete system payloads as well as continuous payloads, such as flexible beams and plates.

XI. REFERENCES

1. Paul, Igor L.; and Bender, Erich K.: Active Vibration Isolation and Active Vehicle Suspension. Report DSR-76109-1, Engineering Projects Laboratory, Department of Mechanical Engineering, Massachusetts Institute of Technology, Cambridge, Massachusetts, November 1, 1966.

2. Erb, Charles G.; and Cox, Sidney S.: The Principles and Analog Studies of an Ideal Vibration Damper. Submitted in partial fulfillment of the requirement for the degree of Master of Science at the Massachusetts Institute of Technology, 1957.

3. Barclay, Ralph G.: An Analog Study of Various Damping Schemes. TR-833, Diamond Ordnance Fuze Laboratories, Ordnances Corps, Washington, D.C., January 30, 1961.

4. Harris, Cyril M.; and Crede, Charles E., eds.: Shock and Vibration Handbook. Vol. II, Chapter 33, McGraw-Hill Book Company, Inc. (New York), c. 1961.

5. Anon: Final Engineering Report on Pneumatic Servo-Controlled Vibration Isolation System for ST-90S and ST-125 Stable Platforms. Repot No. 108, (NASA Contract No. NAS8-5096), Barry Research and Development Corp., Watertown, Massachusetts, May 1964.

6. Freberg, C. R.; and Kemler, E. N.: Elements of Mechanical Vibration. John Wiley and Sons, Inc., 1959.

7. MacDuff, J. N.; and Curreri, J. R.: Vibration Control. McGraw-Hill Book Co., New York, 1958.

8. Doebelin, E. O.: Dynamic Analysis and Feedback Control. McGraw-Hill Book Co., New York, 1962.

9. Lago, G.; and Benningfield, L. M.: Control System Theory. The Ronald Press Co., New York, 1962.

The vita has been removed from the scanned document

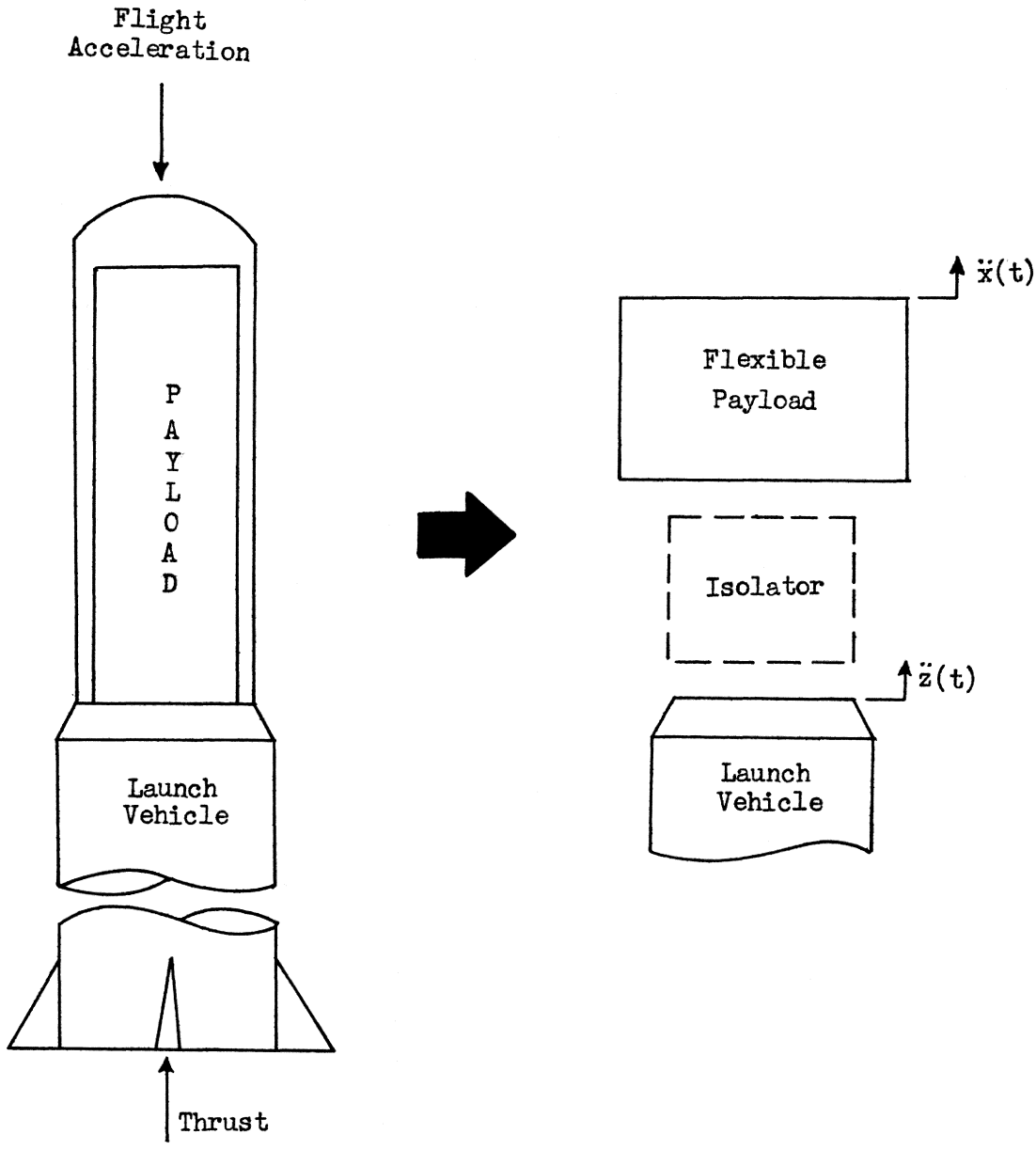

Figure 1.- Schematic diagram of payload vibration isolation problem.

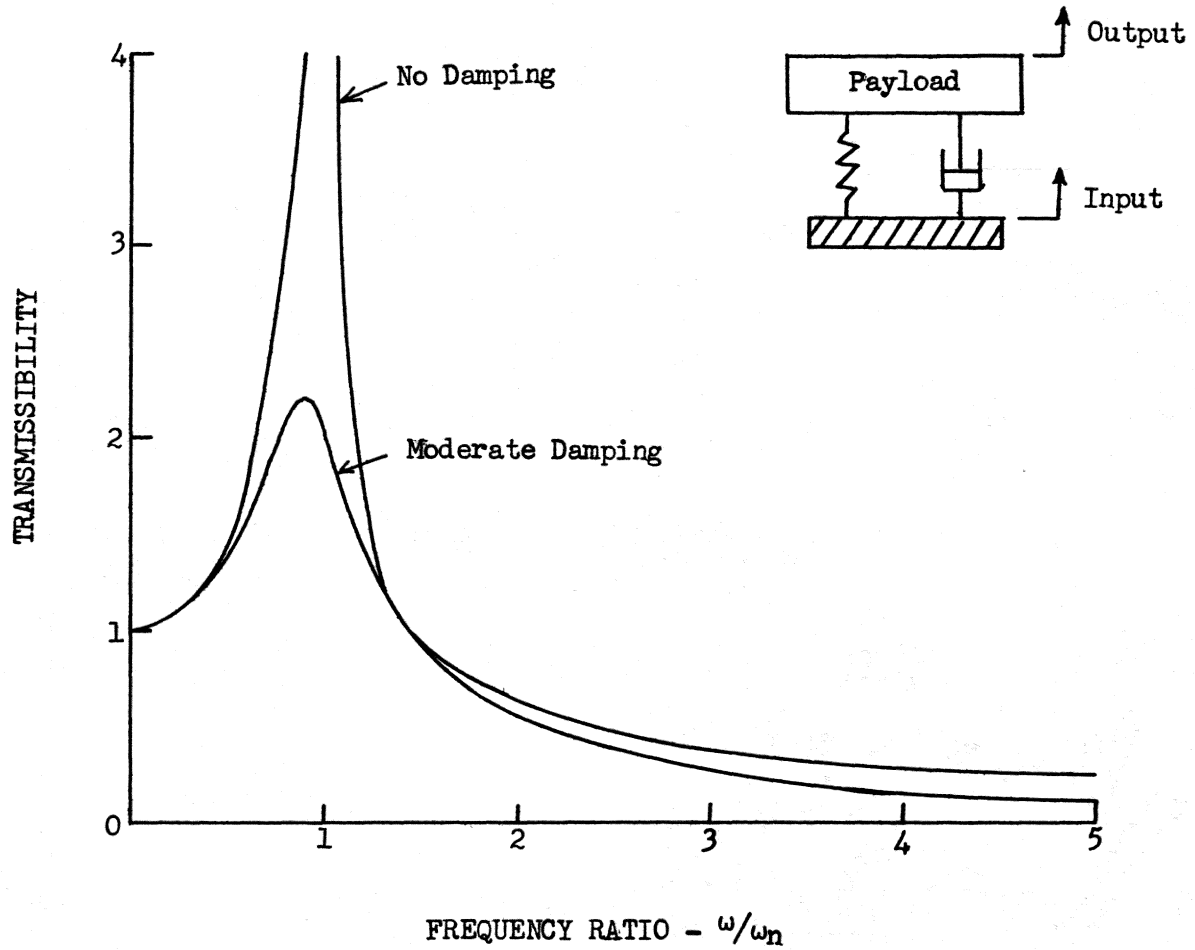

Figure 2.- Conventional passive isolator transmissibility characteristics.

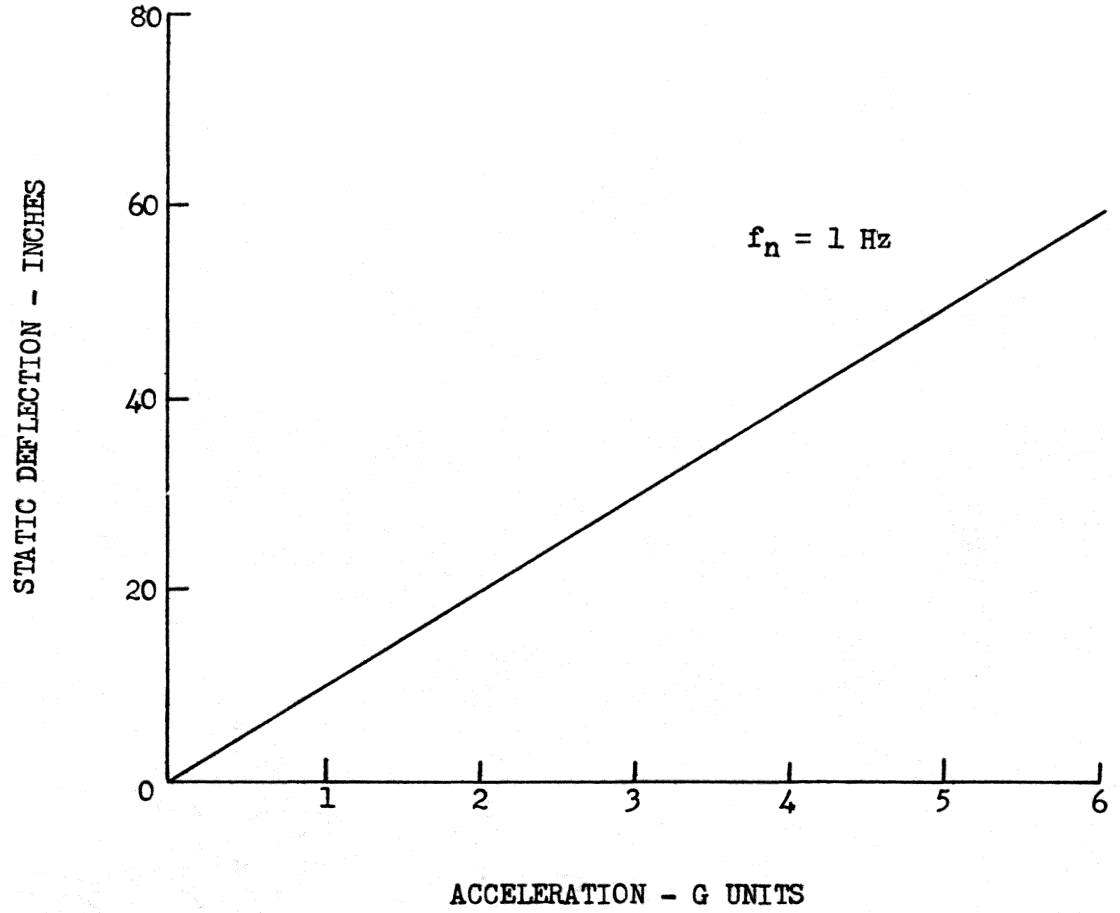

Figure 3.- Variation of static deflection with nondimensional acceleration for a 1-Hz passive isolator.

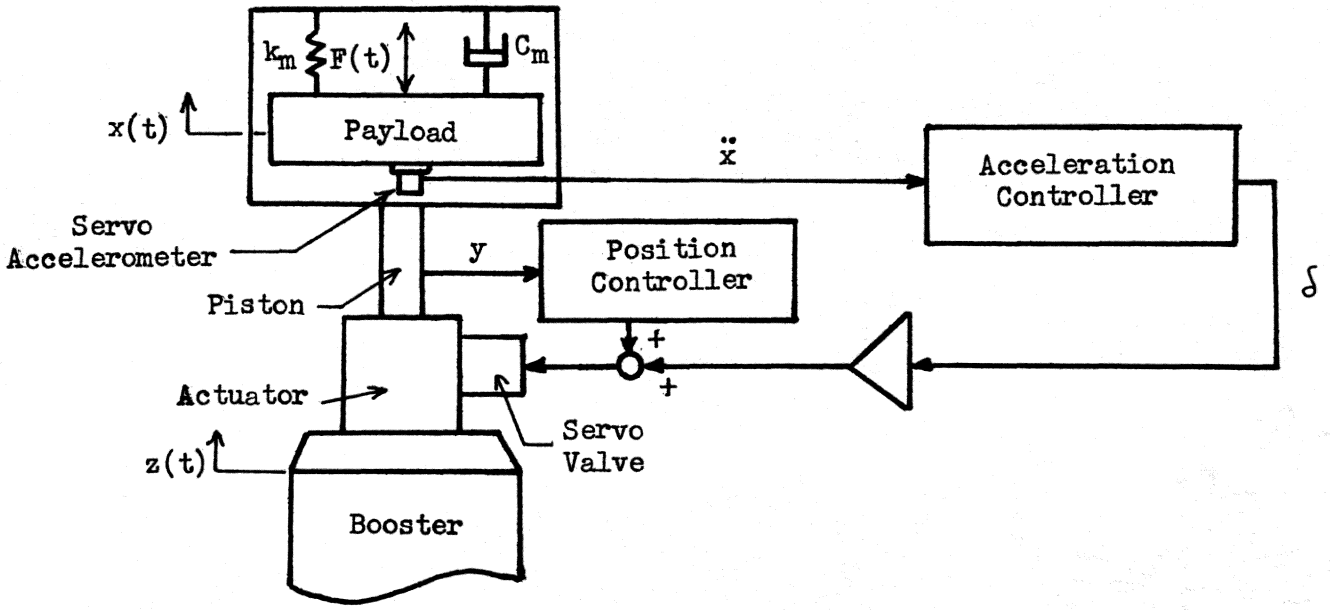

Figure 4.- Schematic diagram of active isolation system.

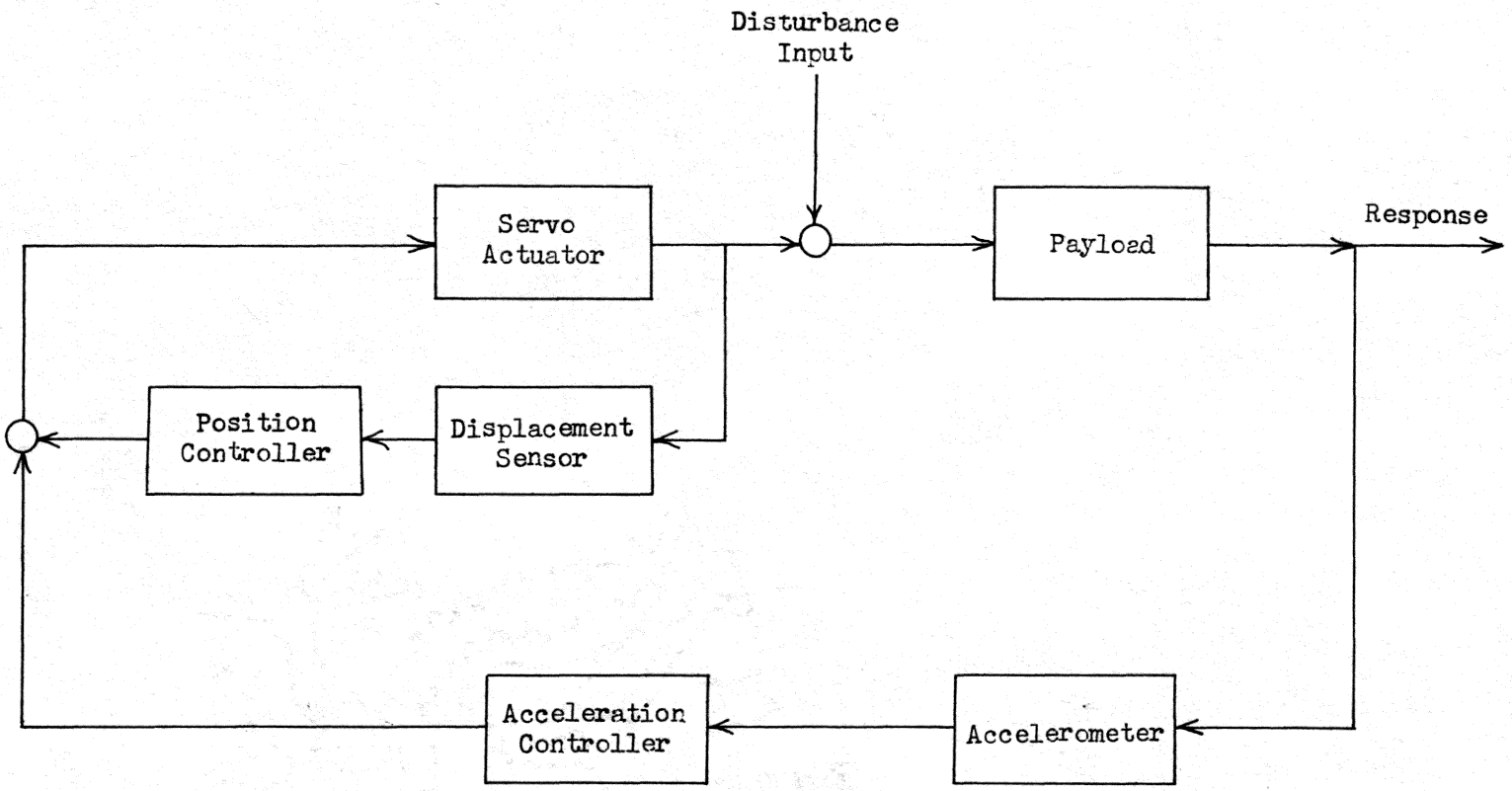

Figure 5.- Signal flow diagram of active isolator-payload system.

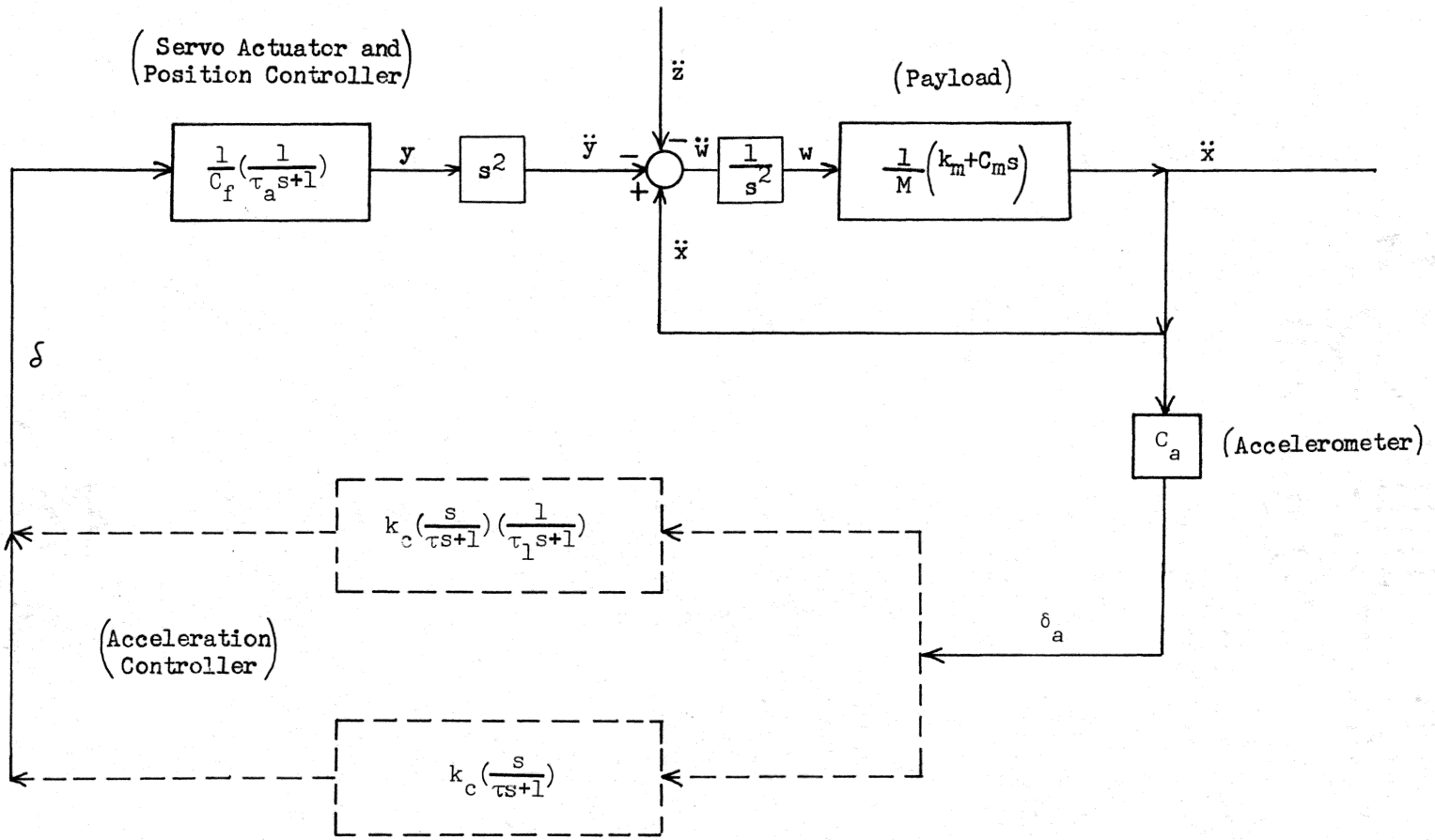

Figure 6.- Block diagram of isolator-payload system (mode I and mode II controllers are mutually exclusive).

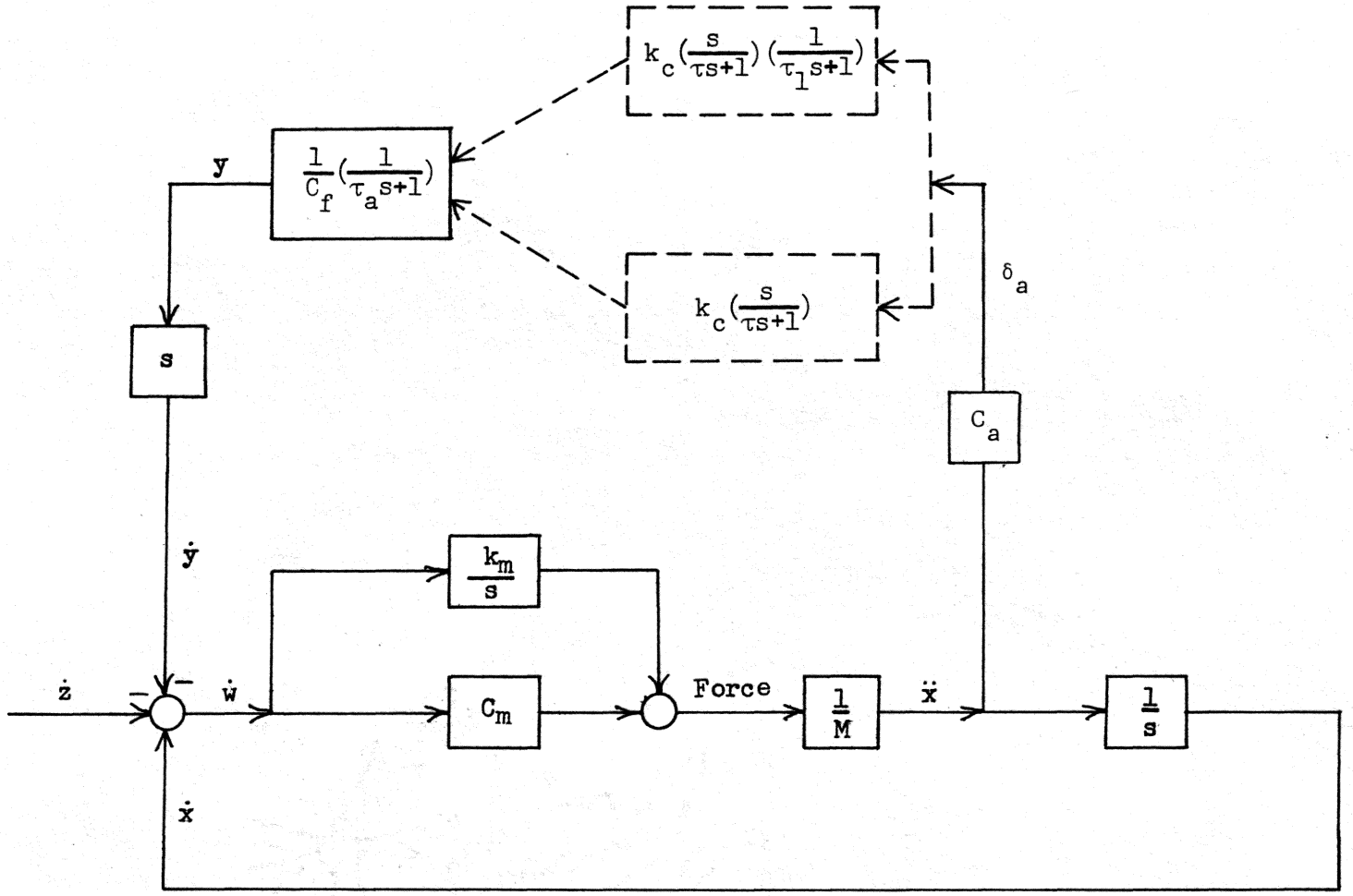

Figure 7.- Block diagram used to develop transmissibility equations.

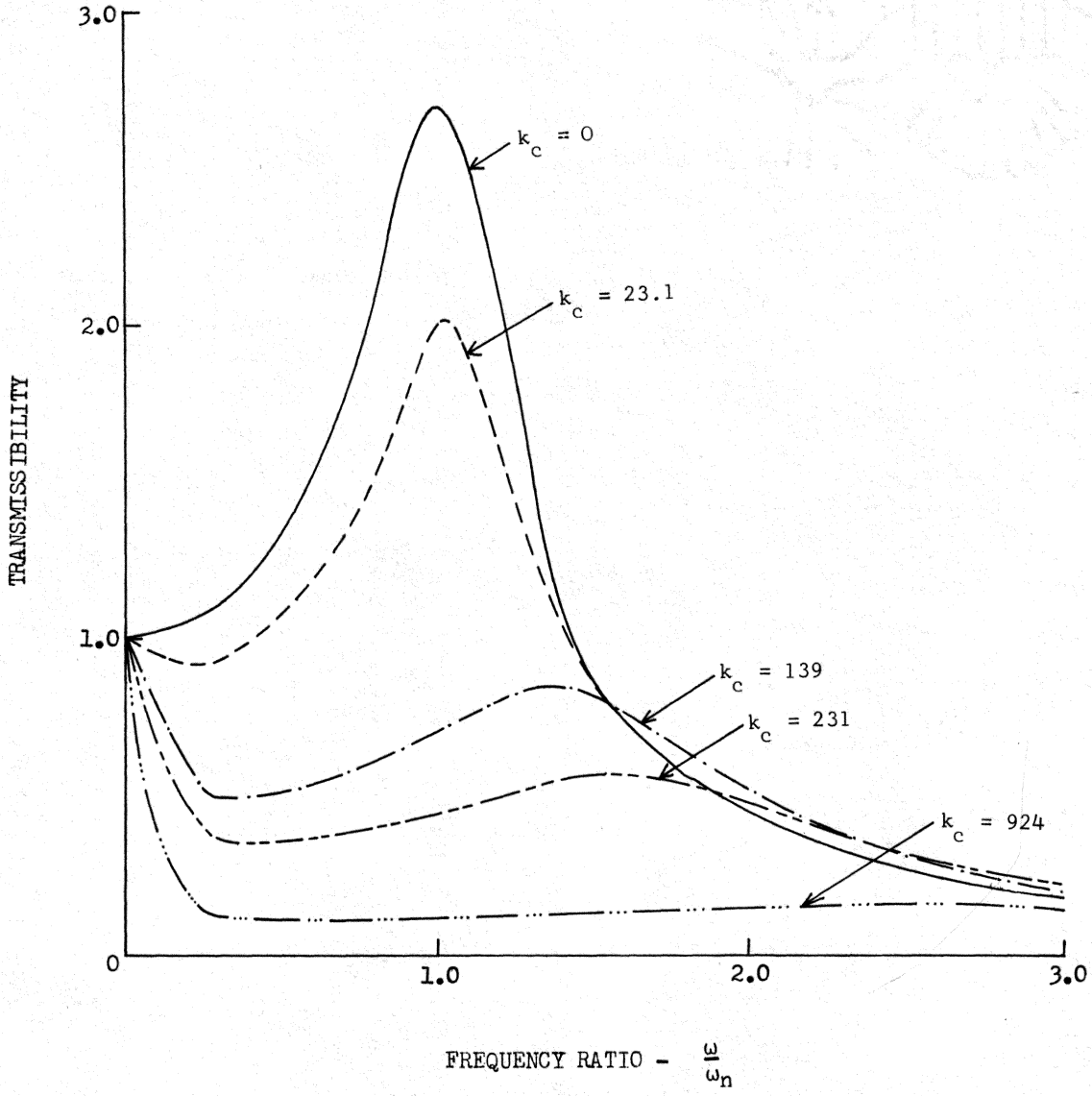

Figure 8.- Variation of transmissibility with frequency ratio for mode I control.

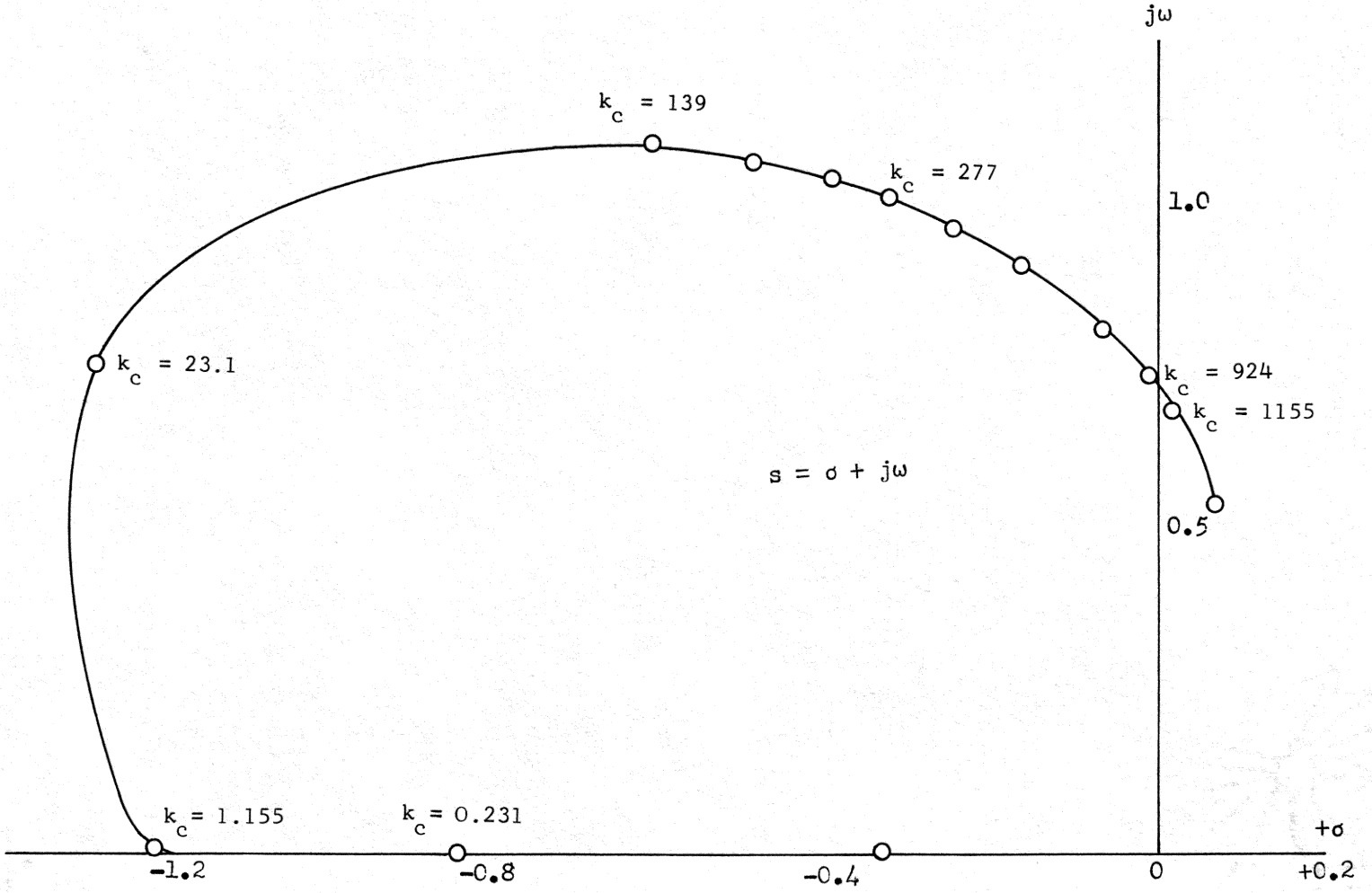

Figure 9.- Root locus for control mode (mode I control).

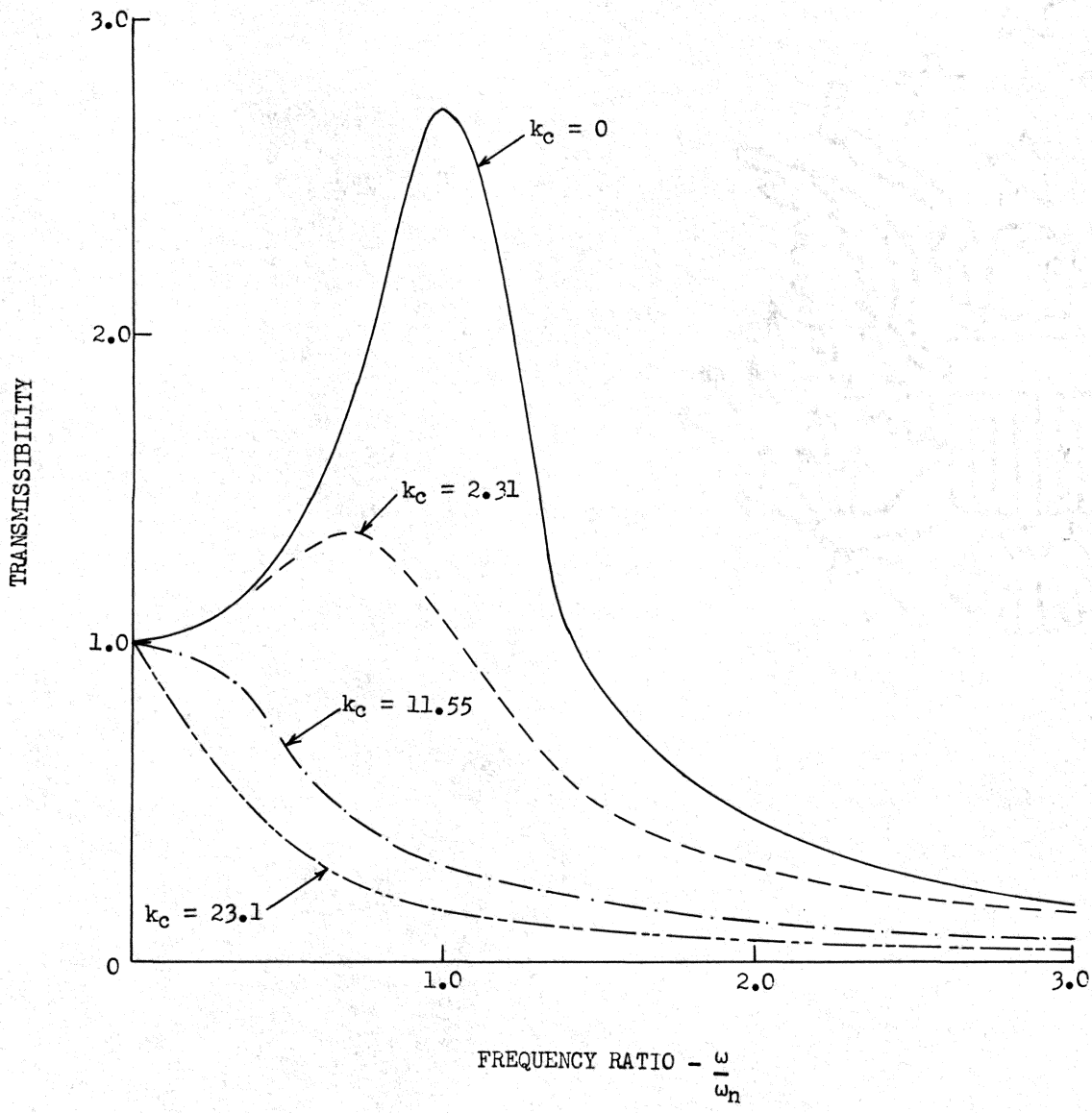

Figure 10.- Variation of transmissibility with frequency ratio for mode II control.

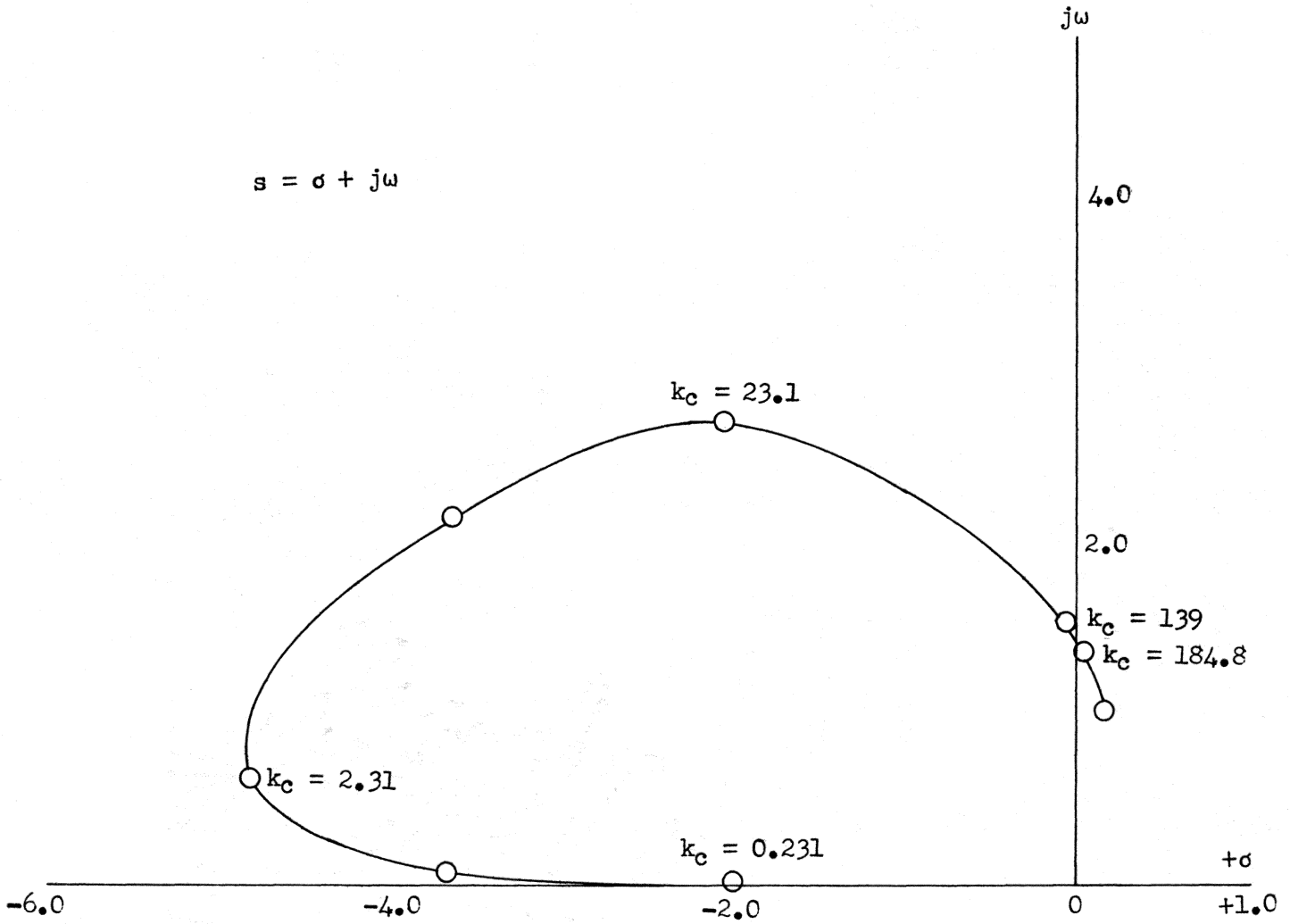

Figure 11.- Root locus for control mode (mode II control).

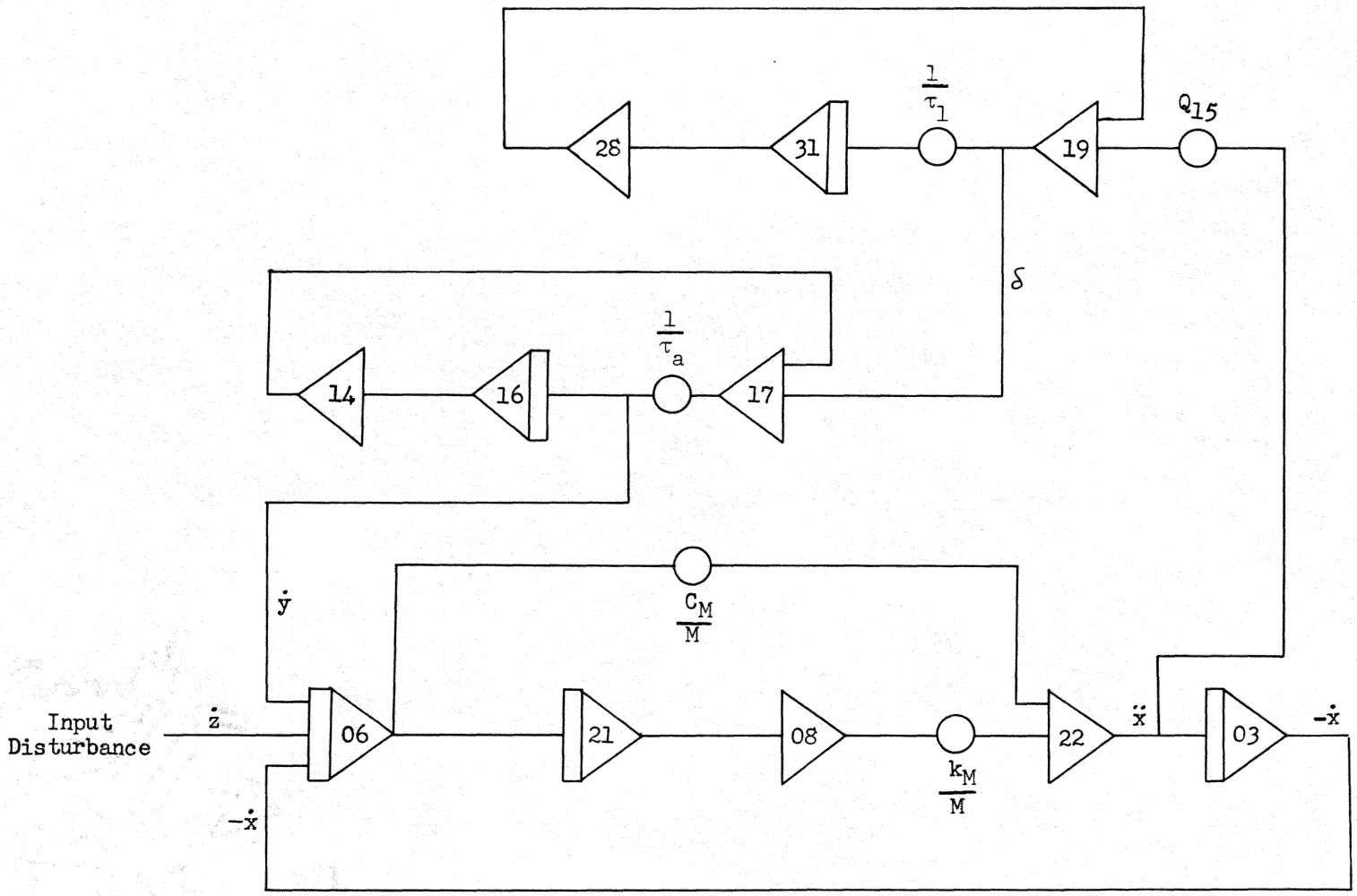

Figure 12.- Analog computer circuit diagram of active isolator-payload system used for transmissibility calculations (mode II control).

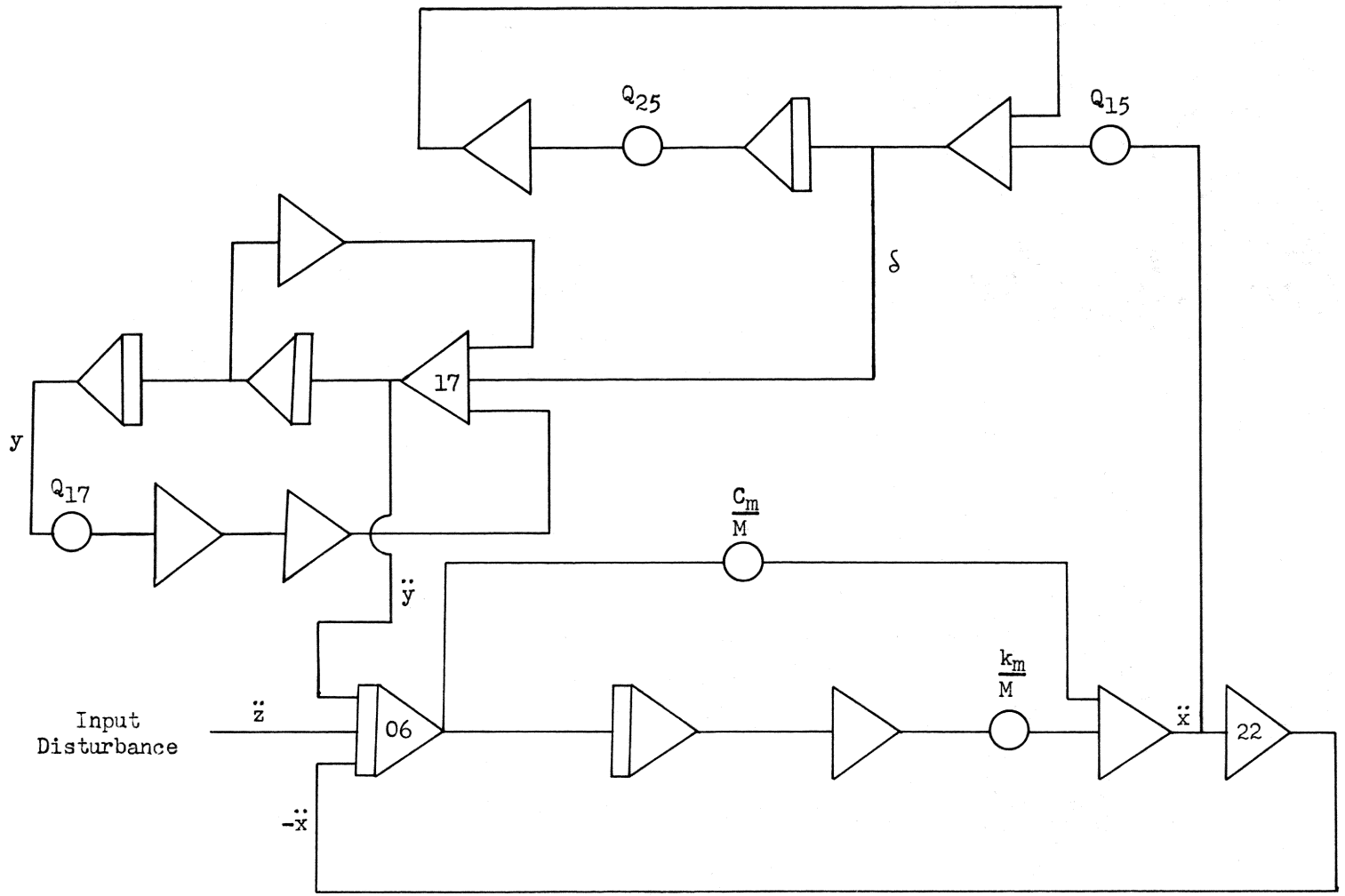

Figure 13.- Analog computer circuit diagram of active isolator-payload system used for transient response study (mode II control).

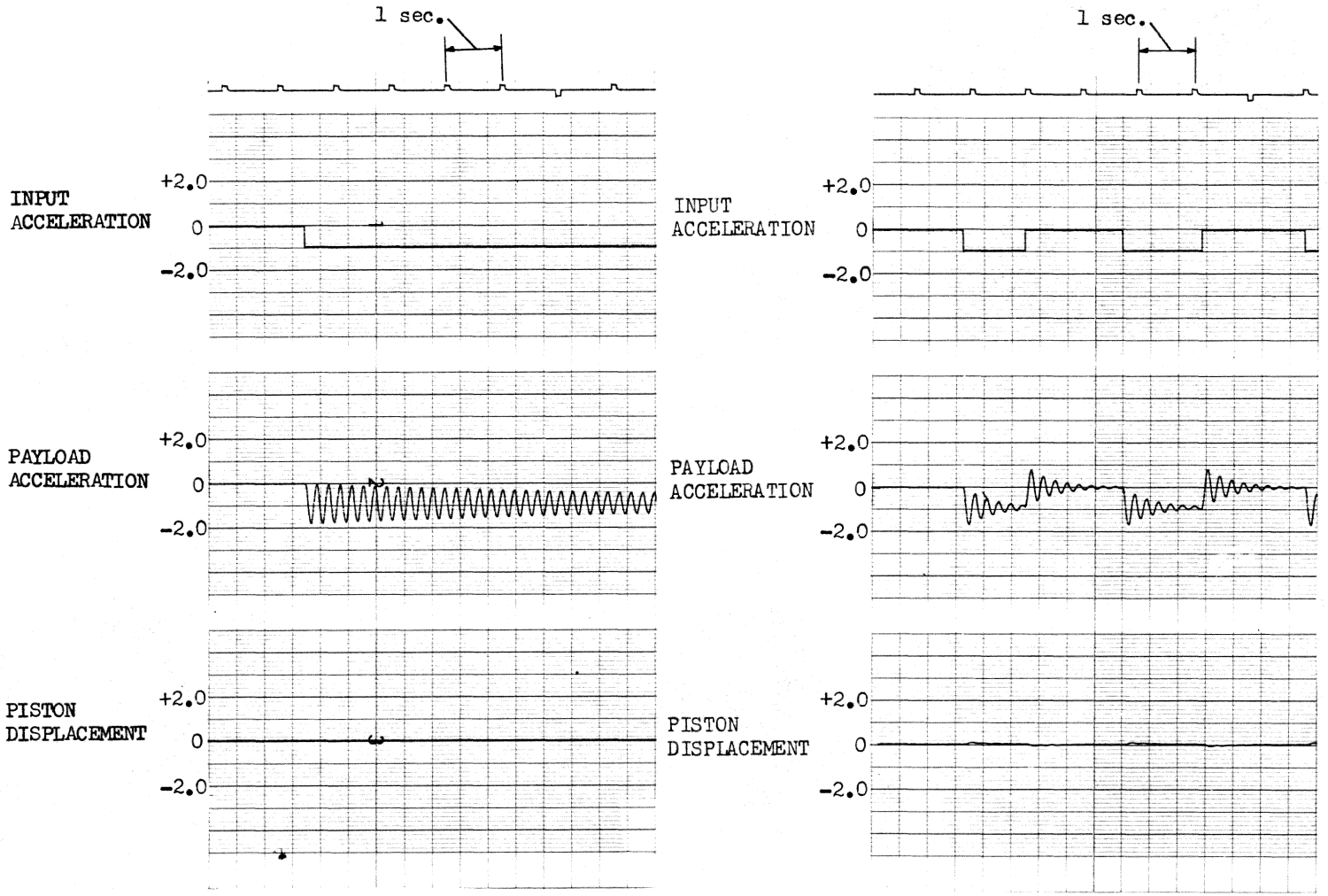

(a) $k_c = 0.$ (b) $k_c = 2.31.$

Figure 14.- Response of payload-isolator system to a 1.0-g step acceleration disturbance.

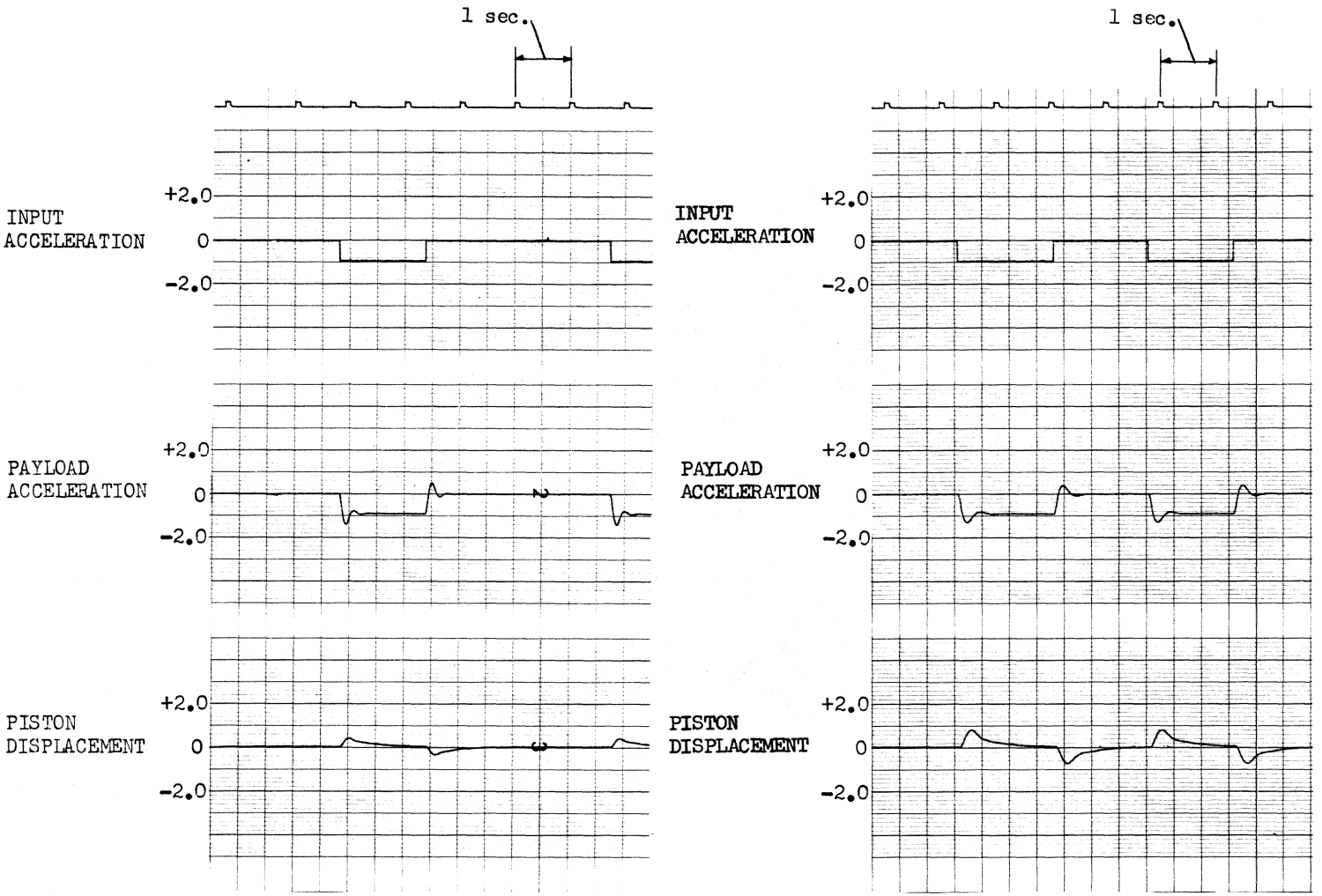

(c) k_c = 11.55.

(d) k_c = 23.1.

Figure 14.- Concluded.

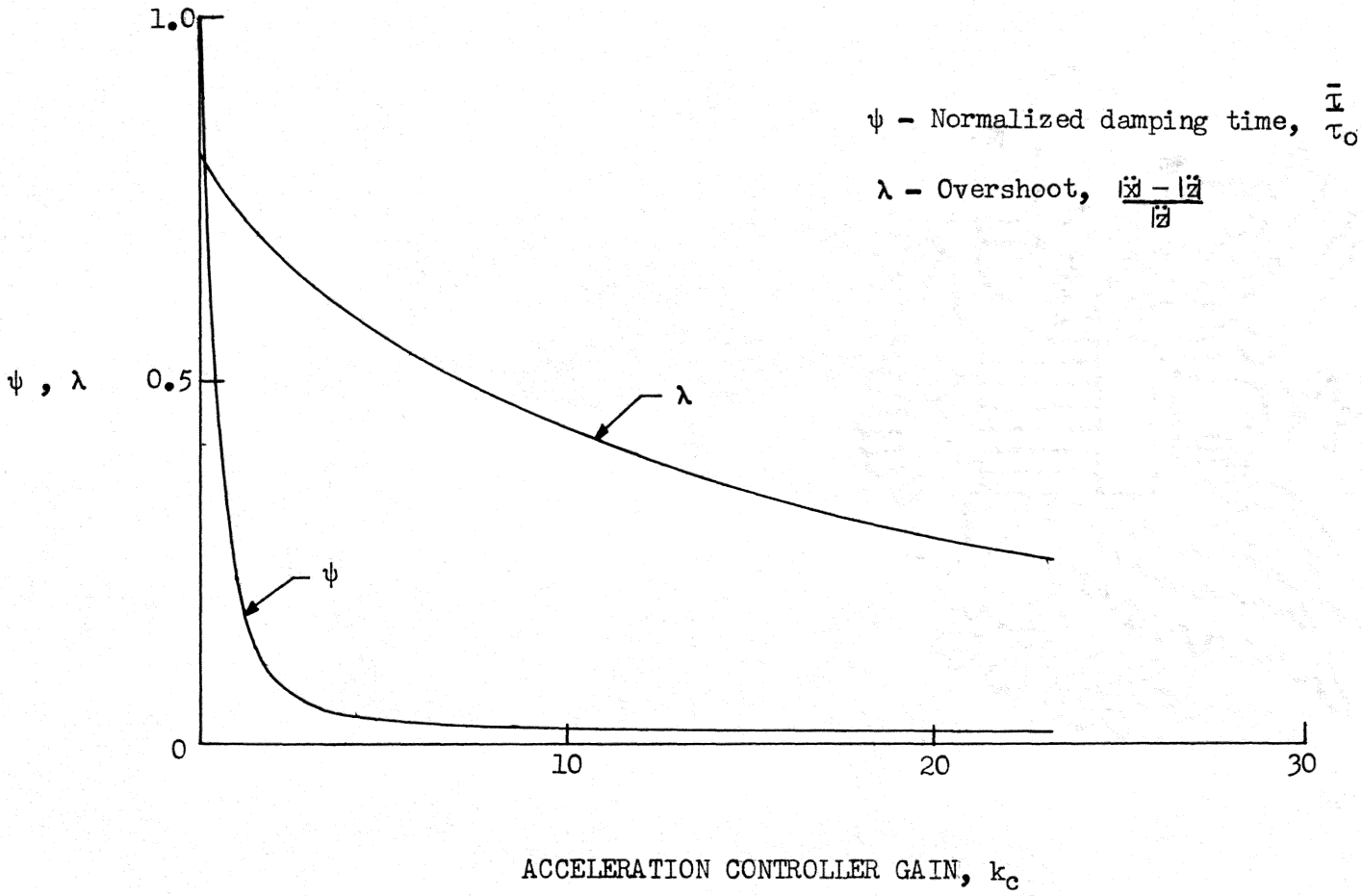

Figure 15.- Variation of normalized damping time and payload overshoot with acceleration feedback gain.

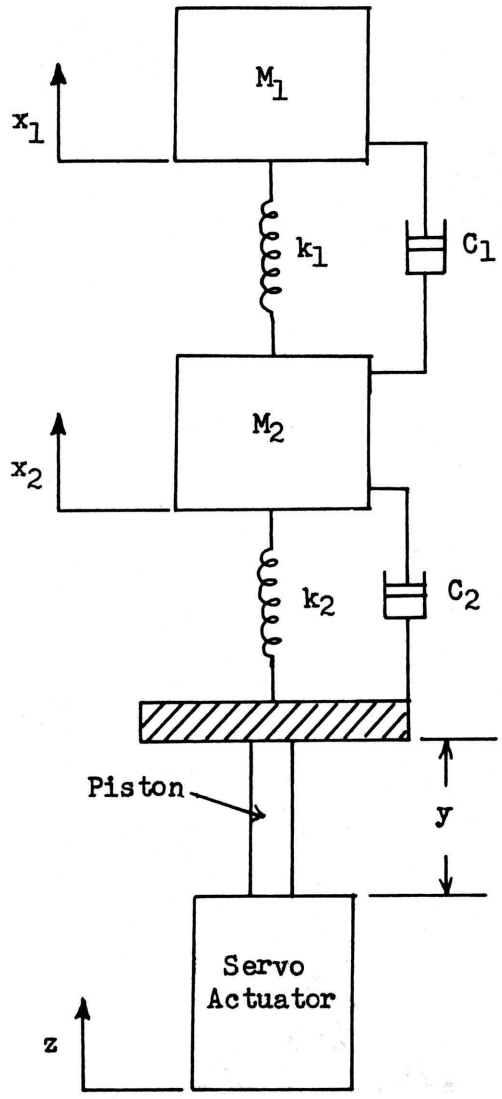

Figure 16.- Two-degree-of-freedom payload model.

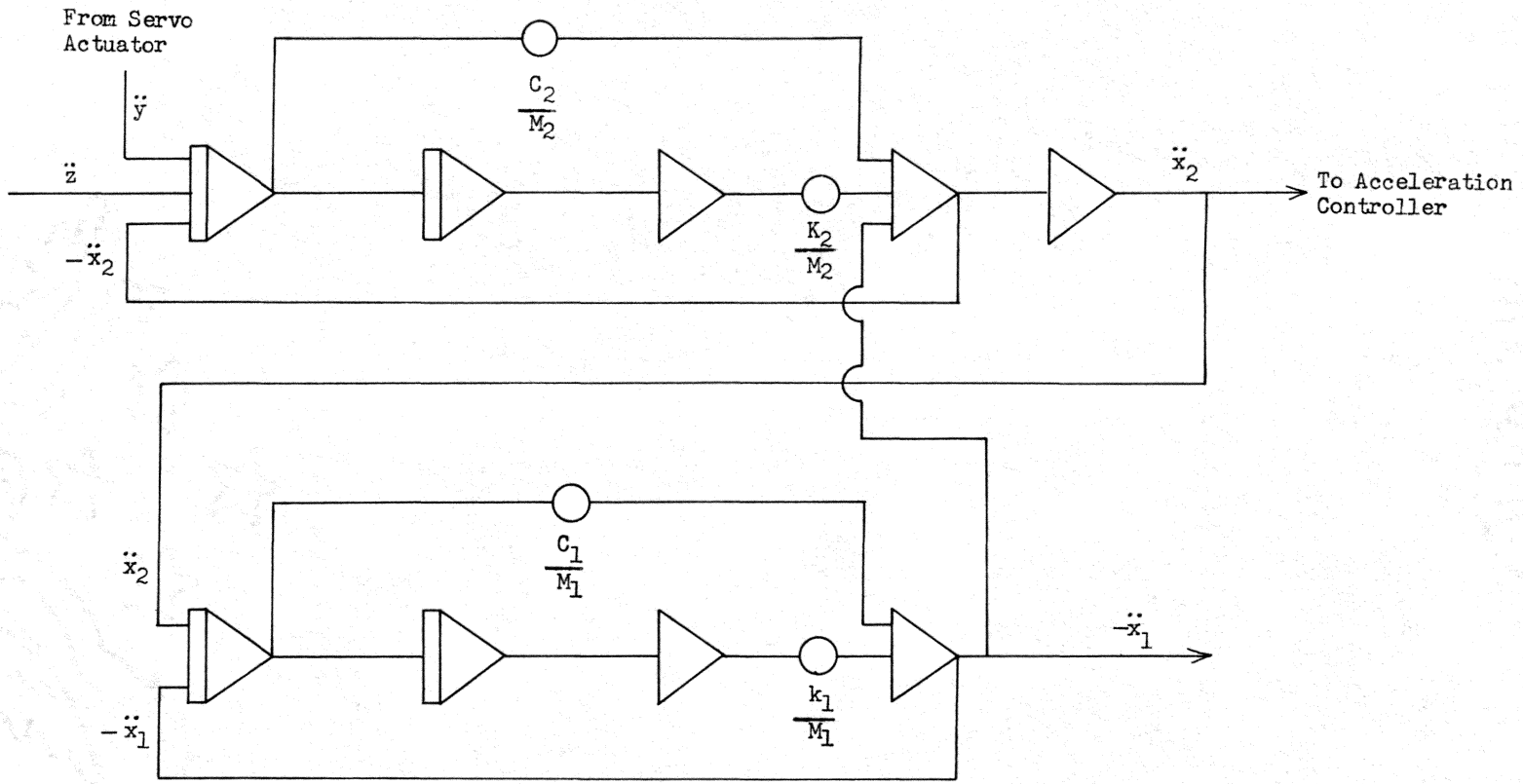

Figure 17.- Analog computer circuit diagram for two-degree-of-freedom payload.

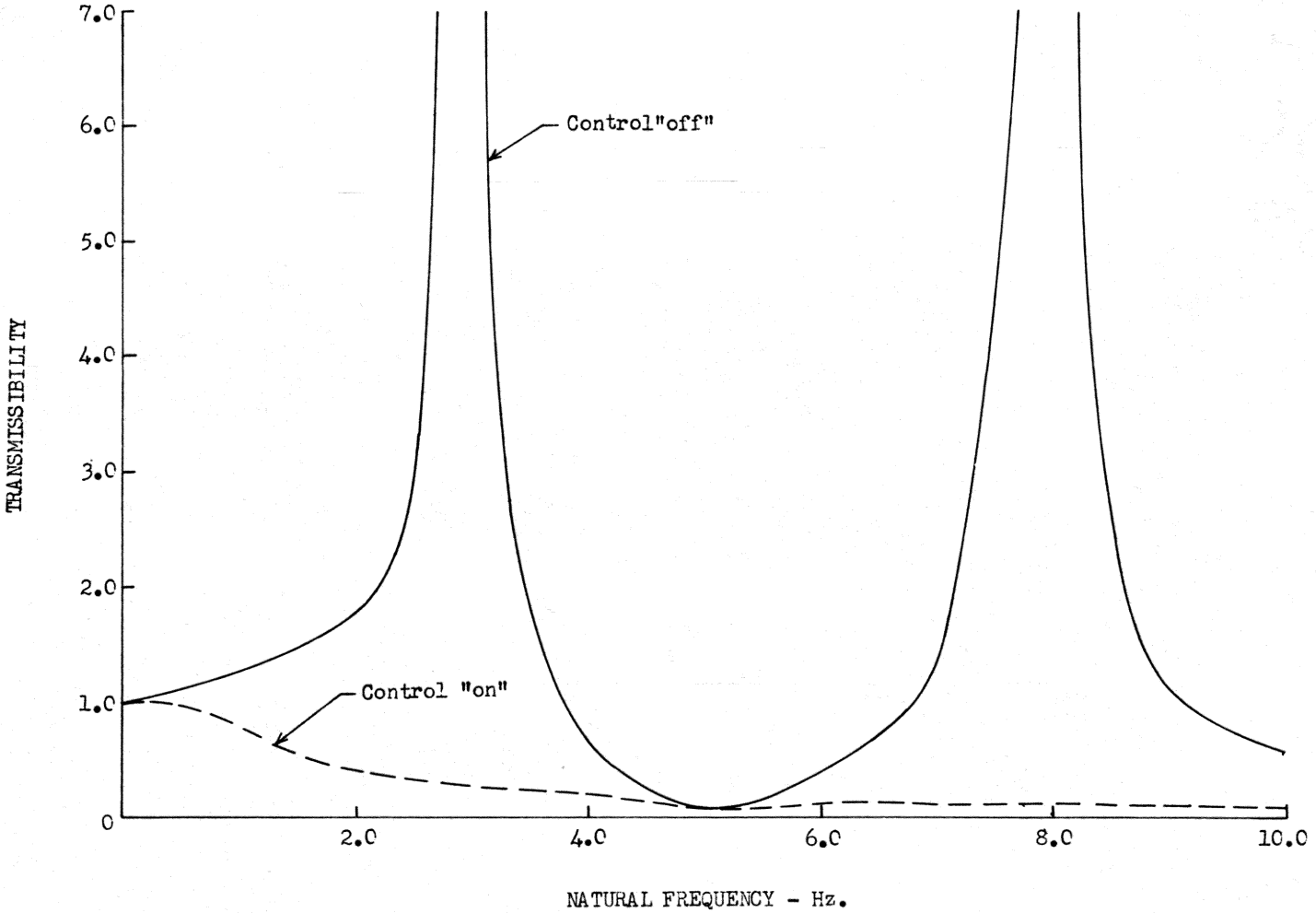

(a) Lower mass, M_2.

Figure 18.- Transmissibility of two-degree-of-freedom payload with active control.

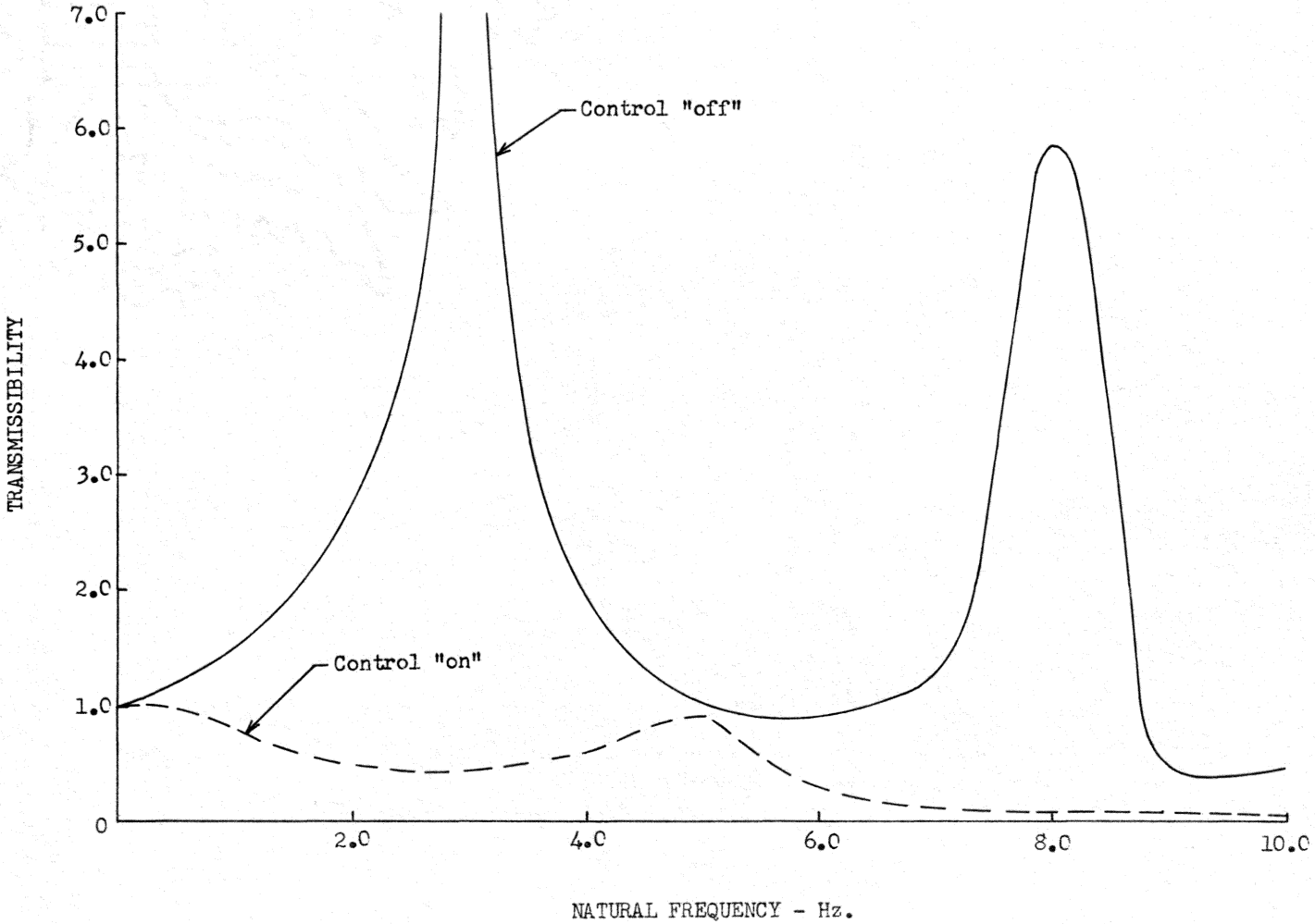

(b) Upper mass, M_1.

Figure 18.- Concluded.

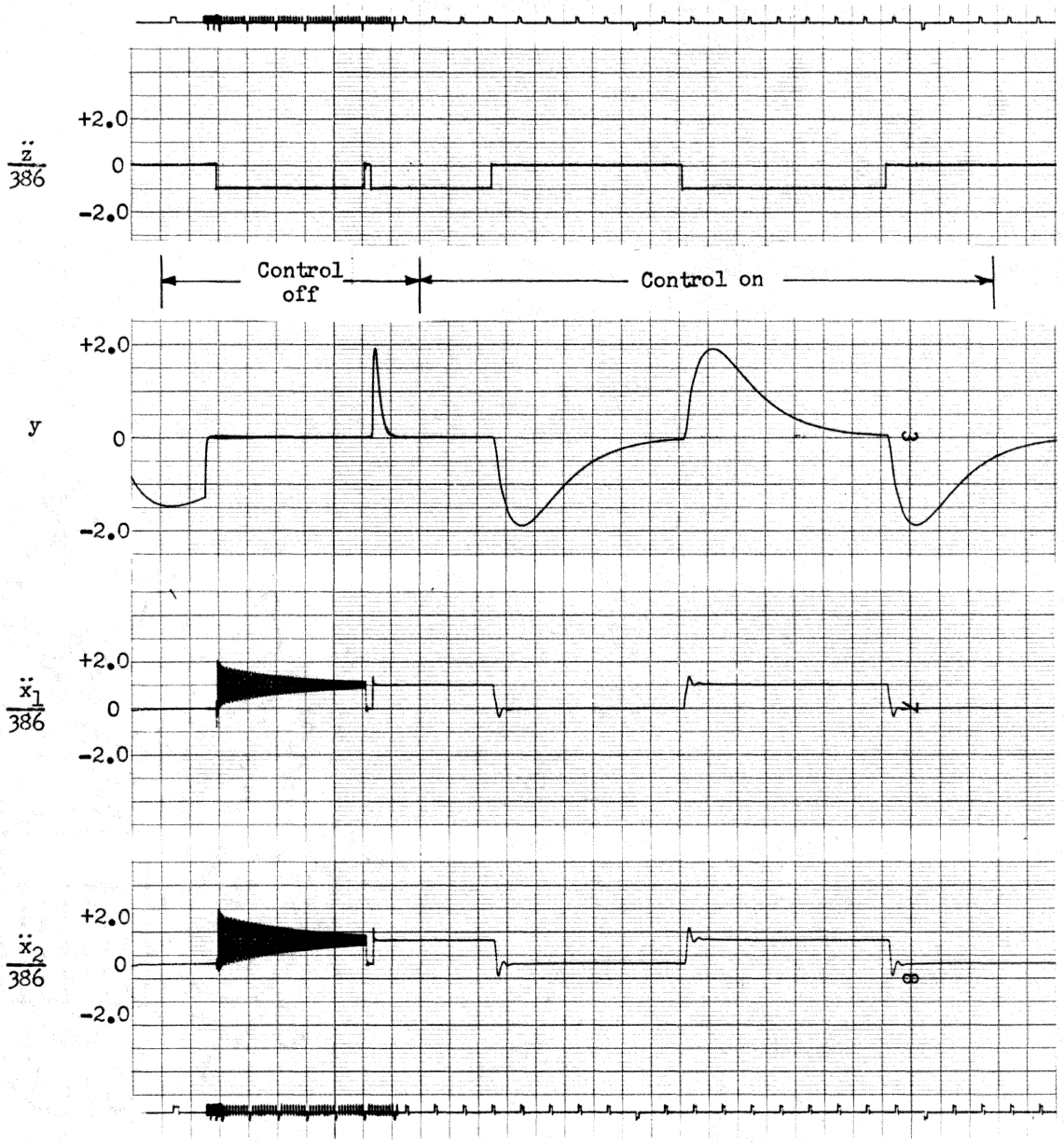

Figure 19.- Response of isolator and two-degree-of-freedom payload to a 1.0-g step input acceleration.

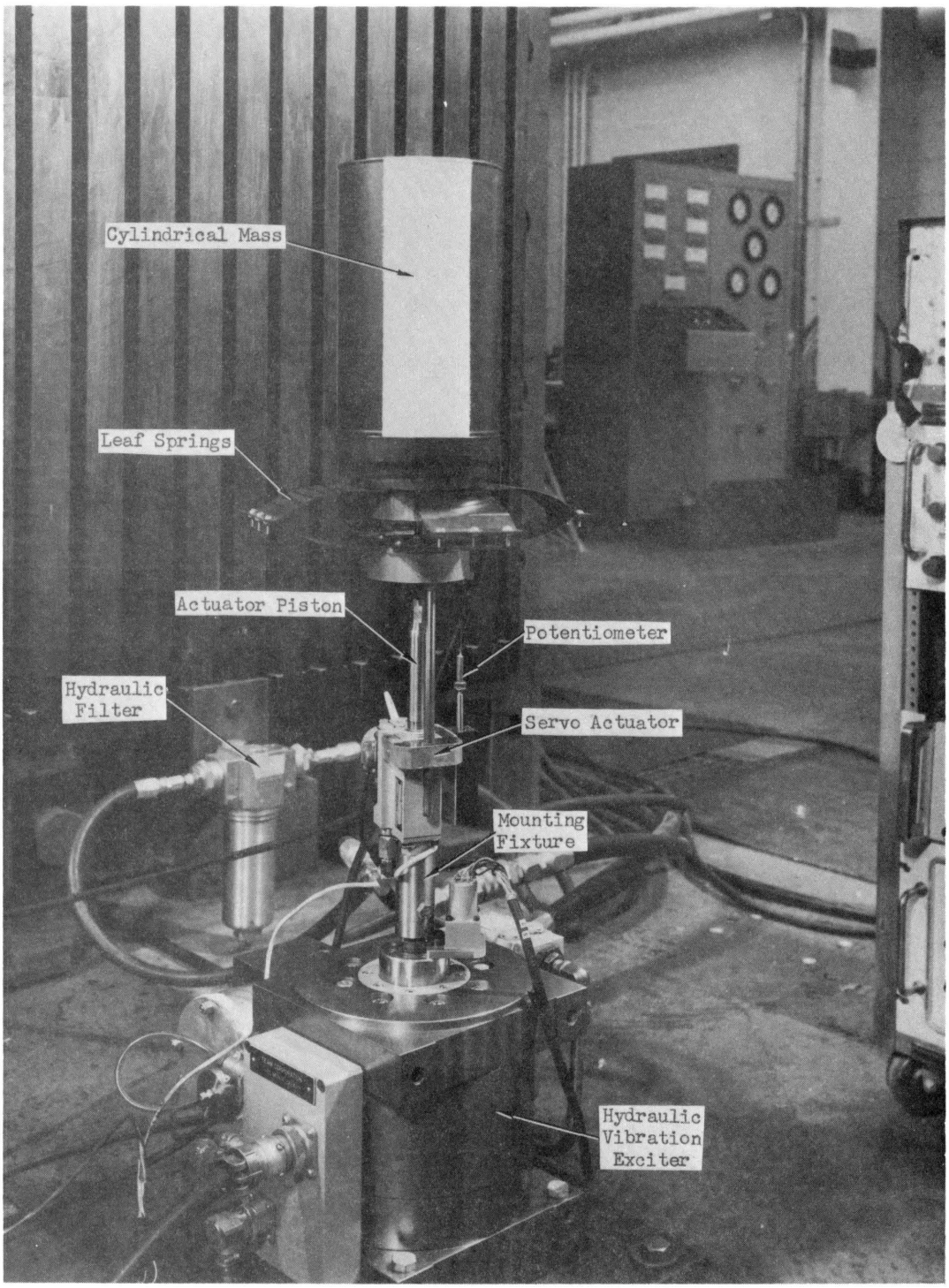

Figure 20.- Photograph of experimental apparatus.

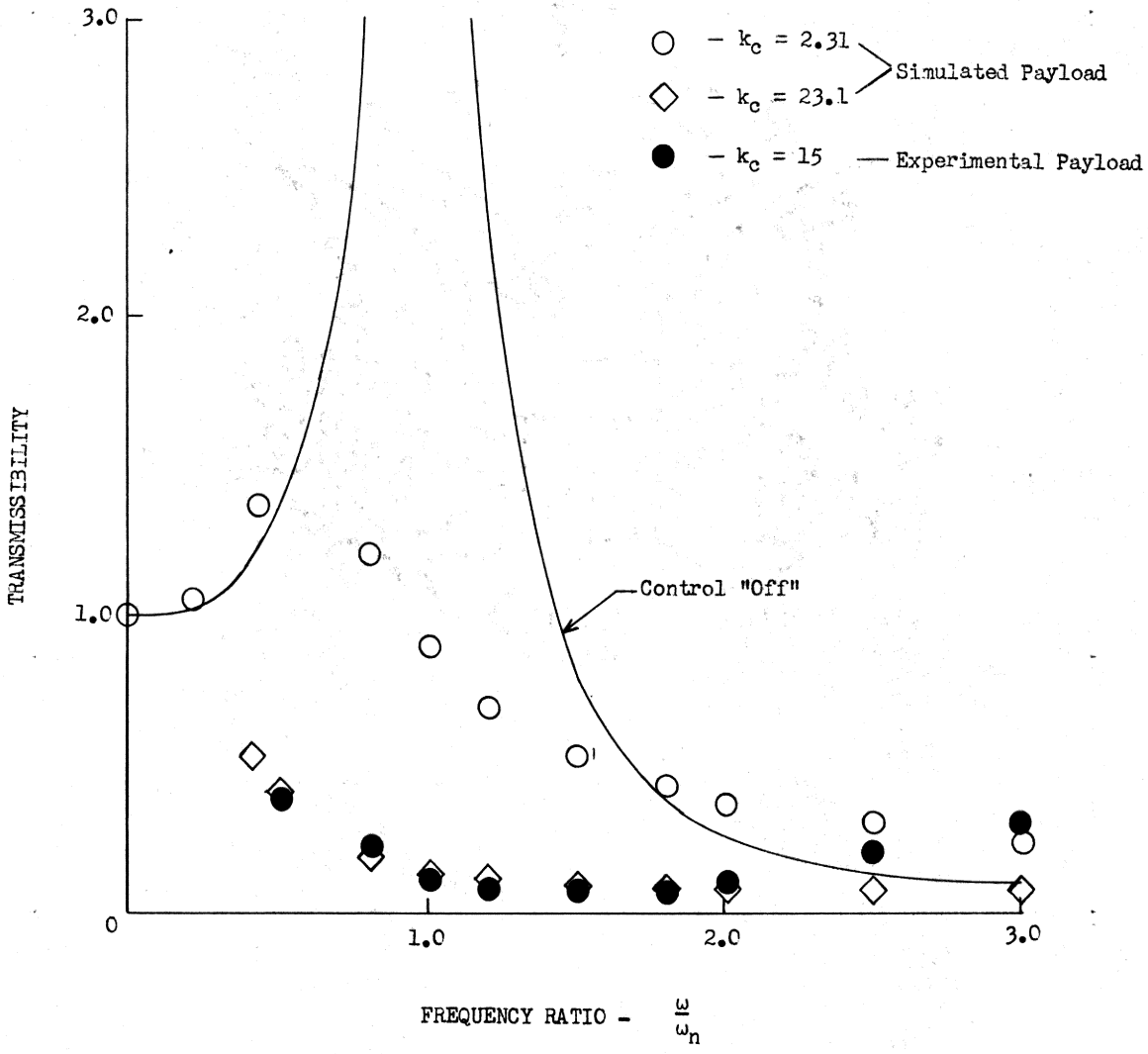

Figure 21.- Variation of transmissibility with frequency ratio for experimental isolator with simulated and experimental payloads.

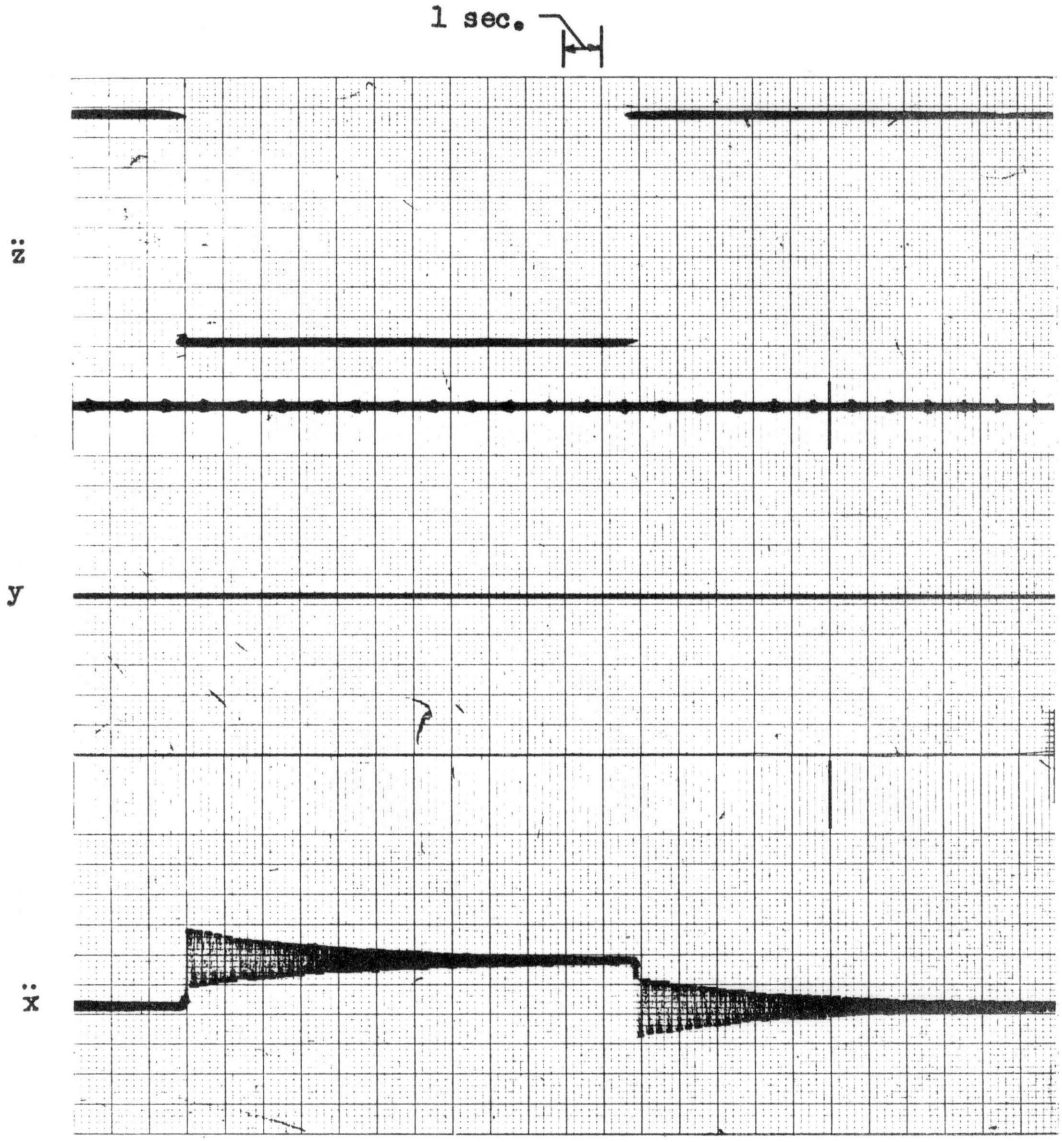

(a) Control off.

Figure 22.- Experimental transient response of simulated payload.

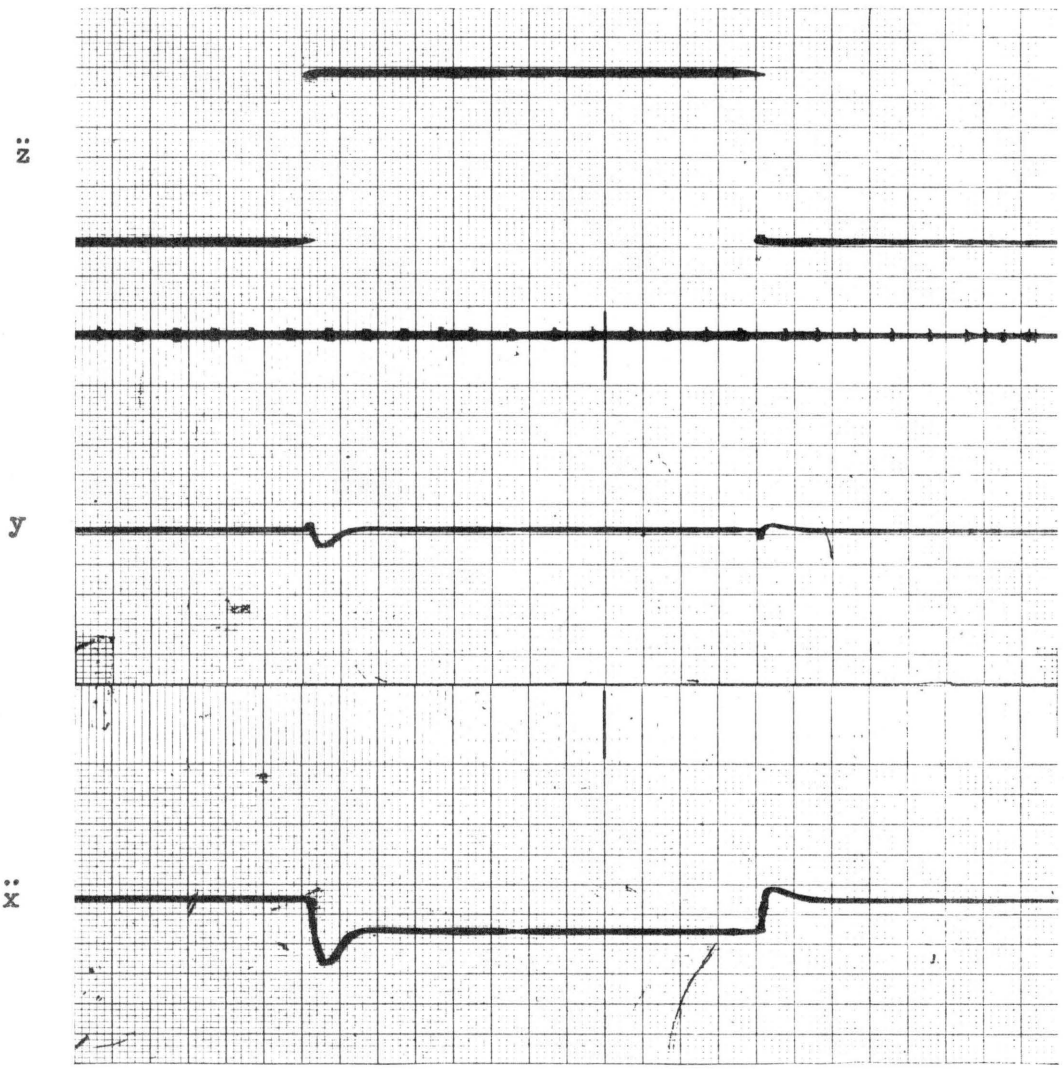

(b) Control on.

Figure 22.- Concluded.

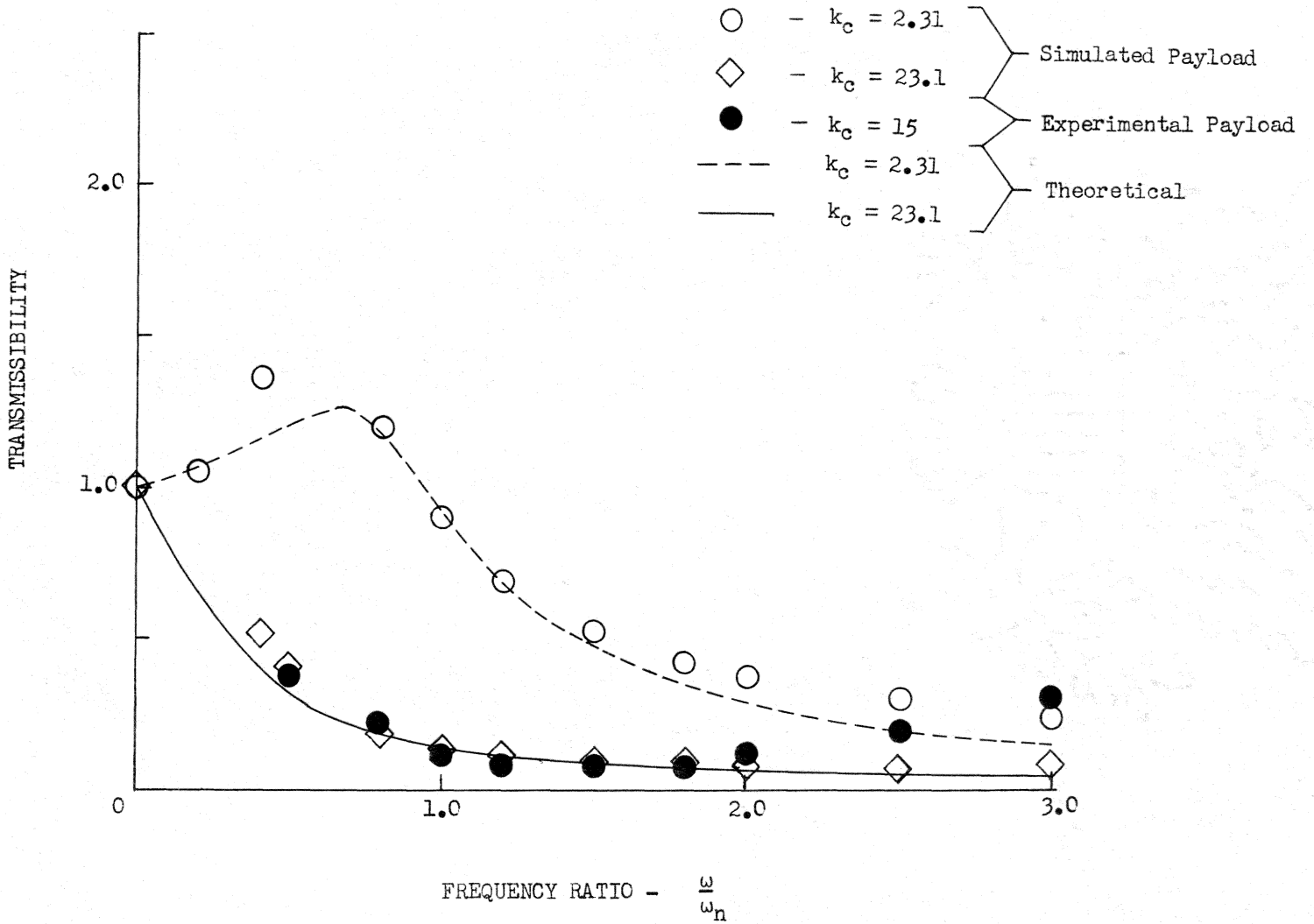

Figure 23.- Comparison of analytical and experimental transmissibility.

ACTIVE VIBRATION ISOLATION FOR FLEXIBLE PAYLOADS

By

Jack D. Leatherwood

ABSTRACT

Results are presented of an experimental and analytical investigation to determine the feasibility of using active control techniques to (1) attenuate the response of a flexible payload to low frequency sinusoidal vibration disturbances, (2) damp the transient response of a flexible payload to step disturbances, and (3) eliminate isolator static deflections under conditions of gradually changing steady acceleration levels. An active vibration isolation system was developed and an experimental working model of the system was built and tested. Digital and analog computer studies were conducted to obtain the transmissibility and transient response characteristics of the isolation system. The analytical and experimental results indicate that the active vibration isolation system is very effective in attenuating the response of a one- and two-degree-of-freedom payload to vibratory disturbances.